Bioorg. Med. Chem. 41 (2021) 116213

Contents lists available at ScienceDirect

Bioorganic & Medicinal Chemistry

journal homepage: www.elsevier.com/locate/bmc

Computer-aided design of 1,4-naphthoquinone-based inhibitors targeting cruzain and rhodesain cysteine proteases

Leandro Rocha Silva [a,b], Ari Souza Guimarães [a,b], Jadiely do Nascimento [b], Igor José do Santos Nascimento [a], Elany Barbosa da Silva [c], James H. McKerrow [c], Sílvia Helena Cardoso [b], Edeildo Ferreira da Silva-Júnior [a,*]

[a] Chemistry and Biotechnology Institute, Federal University of Alagoas, Campus A.C. Simões, Lourival Melo Mota Avenue, Maceió 57072-970, Brazil
[b] Laboratory of Organic and Medicinal Synthesis, Federal University of Alagoas, Campus Arapiraca, Manoel Severino Barbosa Avenue, Arapiraca 57309-005, Brazil
[c] Center for Discovery and Innovation in Parasitic Diseases, Skaggs School of Pharmacy and Pharmaceutical Sciences, University of California San Diego, La Jolla, CA, USA

ARTICLE INFO

Keywords:
Naphthoquinone
Drug design
Cysteine protease
MM-PBSA
DFT

ABSTRACT

Chagas disease and Human African Trypanosomiasis (HAT) are caused by *Trypanosoma cruzi* and *T. brucei* parasites, respectively. Cruzain (CRZ) and Rhodesain (RhD) are cysteine proteases that share 70% of identity and play vital functions in these parasites. These macromolecules represent promising targets for designing new inhibitors. In this context, 26 CRZ and 5 RhD 3D-structures were evaluated by molecular redocking to identify the most accurate one to be utilized as a target. Posteriorly, a virtual screening of a library containing 120 small natural and nature-based compounds was performed on both of them. In total, 14 naphthoquinone-based analogs were identified, synthesized, and biologically evaluated. In total, five compounds were active against RhD, being three of them also active on CRZ. A derivative of 1,4-naphthoquinonepyridin-2-ylsulfonamide was found to be the most active molecule, exhibiting IC_{50} values of 6.3 and 1.8 μM for CRZ and RhD, respectively. Dynamic simulations at 100 ns demonstrated good stability and do not alter the targets' structures. MM-PBSA calculations revealed that it presents a higher affinity for RhD (-25.3 Kcal mol^{-1}) than CRZ, in which van der Waals interactions were more relevant. A mechanistic hypothesis (via C3-Michael-addition reaction) involving a covalent mode of inhibition for this compound towards RhD was investigated by covalent molecular docking and DFT B3LYP/6–31 + G* calculations, exhibiting a low activation energy ($\Delta G^{\ddagger}$) and providing a stable product (ΔG), with values of 7.78 and − 39.72 Kcal mol^{-1}, respectively; similar to data found in the literature. Nevertheless, a reversibility assay by dilution revealed that **JN-11** is a time-dependent and reversible inhibitor. Finally, this study applies modern computer-aided techniques to identify promising inhibitors from a well-known chemical class of natural products. Then, this work could inspire other future studies in the field, being useful for designing potent naphthoquinones as RhD inhibitors.

1. Introduction

Trypanosoma cruzi and *T. brucei* are parasites that belong to the *Trypanosomatidae* family responsible for Chagas and Human African Trypanosomiasis - HAT (also named sleeping sickness disease), respectively. Chagas disease is transmitted to humans through the bite of infected blood-sucking *Triatomine* insects during their meal and blood transfusion, while HAT is transmitted by tsetse flies.[1–3] *T. brucei* presents two subspecies, *T. brucei rhodesiense* and *T. brucei gambiense*, responsible for different symptoms.[4,5] Million people are infected worldwide, and other millions are living at risk zones of infection, mostly in Latin America. There are only two drugs to treat Chagas disease, nifurtimox and benznidazole (Figure 1), both of these were introduced in the 1970 s, and these are associated with resistance cases and numerous side effects that make treatment difficult.[6,7] For HAT, suramin and pentamidine (Figure 1) are prescribed for the early stage, presenting severe side effects. Also, melarsoprol (Figure 1), a toxic derivative from arsenic, can cause encephalopathies in the late stage of the disease.[4,5] Besides, the current treatments are highly inefficient due to the low effectiveness of them.[8] Additionally, fexinidazole and eflornithine (Figure 1) have been

* Corresponding author. Tel.: +55 82 9 9610 8311.
E-mail address: edeildo.junior@iqb.ufal.br (E.F. da Silva-Júnior).

https://doi.org/10.1016/j.bmc.2021.116213
Received 26 February 2021; Received in revised form 23 April 2021; Accepted 5 May 2021
Available online 11 May 2021

used to treat infections caused by *T. brucei gambiense* in humans.[9–12] Consequently, there is a crucial need for the development of new drugs that would ideally be affordable, safe, and effective to treat these Neglected Tropical Diseases (NTDs). In general, trypanosomiasis has two clinic phases, being acute or chronic. The acute stage is asymptomatic, although 10–50% of patients die during this phase. In the chronic stage, 20% of patients develop digestive problems, heart diseases, and even neurological disorders.[13–15]

T. cruzi life cycle involves amastigote, trypomastigote, and epimastigote forms. Trypomastigote forms that circulate in the host's blood are converted into epimastigote forms, after the ingestion of blood by insect vectors. Subsequently, these forms proliferate and differentiate into metacyclic forms, which are released in feces, being able to start a new infection cycle.[2,16] Similarly, *T. brucei* life cycle alternates between a mammalian host, which presents slender, intermediate, and stumpy forms, and tsetse fly when stumpy forms are converted into procyclic forms, proliferate migrating to epimastigote forms, and developing in metacyclic forms into salivary gland.[17] For parasite's survival, the major cysteine proteases from *T. cruzi* and *T. brucei*, cruzain (CRZ) and rhodesain (RhD), respectively; play essential functions involved in the host invasion process and shares 70% identity, providing an attractive target for the development of a broad-spectrum inhibitor for both disease.[3,18]

CRZ represents the largest cysteine protease from *T. cruzi*, and it is associated with several biological processes into the parasite, such as differentiation, invasion, and proliferation in host cells.[19–21] Biochemical studies involving animal models suggest that CRZ is the primary target of infection control and parasite elimination.[22,23] CRZ is a cathepsin L-like protein from the papain family.[24] Similarly, RhD (or *T. brucei* cathepsin L) is the largest cysteine protease from *T. brucei*, and it belongs to the papain-like subfamily, Clan CA family C1.[25,26] Moreover, it is related to protein degradation and intracellular transport of proteins between the insect and host cells.[25] CRZ and RhD have four main subsites for ligands (S1′, S1, S2, and S3), in which the S2 subsite is the specific site with low solvent accessibility and responsible for interactions with hydrophobic and basic groups.[24] The active site is located between two domains, with the catalytic triad (Cys^{25}, His^{159}, and Asn^{175} for CRZ, and Cys^{25}, His^{162}, and Asn^{182} for RhD).[24,27,28] The nucleophilic residue $Cys(S^-)$ is capable of attacking carbonyl groups with fissile amide bonds.[29,30] Finally, both of these enzymes are present in all stages of the parasite's life cycle (epimastigotes, trypomastigotes, metacyclic trypomastigotes, and amastigotes), making them excellent targets to be explored in the discovery of drugs against these NTDs.[24,31]

In folk medicine, vegetal species containing 1,4-naphthoquinones have been utilized for the treatment of many diseases,[32] representing a valuable source for new drugs.[33,34] 1,4-Naphthoquinones are present in several plant families, including *Bignoniaceae* and *Verbenaceae*, and even fungi and insects. 1,4-Naphthoquinone-based compounds are also able to exert activity upon the different targets by diverse mechanisms, including oxidative stress and direct interaction with cellular macromolecules.[35–37] Notwithstanding these facts, this natural product class is mainly known for interfering in the biological redox balance. In this context, the redox cycle of quinones can be initiated by one-electron reduction that leads to the formation of semiquinones.[16,38–40] Then, these compounds can covalently bind to nucleic acids and proteins, inactivating them.[41] Alternatively, another mechanism is reducing quinones by two-electrons, mediated by DT-diaphorase, resulting in the formation of hydroquinones. These molecules can disrupt the electron transport chain, intercalate with DNA, uncouple oxidative phosphorylation, and produce reactive oxygen species (ROS).[16,38–40]

Some studies have revealed that naphthoquinone analogs exhibit diverse biological properties, including anticancer activity by inhibiting topoisomerase II and telomerase through DNA alkylation or interaction, and via inhibition of the heat shock protein HSP90.[42] Also, naphthoquinones have been reported to inhibit the recombinant falcipain 2 *in vitro*, a cysteine protease from *Plasmodium falciparum*.[37] Among other activities, 1,4-naphthoquinone-based compounds have been demonstrated to act as trypanocidal agents. In this context, lapachol and β-lapachone are naphthoquinone derivatives extracted from trees from the *Tabebuia* genus, which indigenous people have used to treat many parasitic infections. Nonetheless, these have not become drugs, but they have been extensively explored in medicinal chemistry to seek new trypanocidal compounds yet since these are considered privileged scaffolds.[43–45] Then, Salas *et al.*[41] determined the activity of lapachol, α-lapachone, and β-lapachone (Figure 2) toward amastigotes and trypomastigotes of *T. cruzi* Tulahuén strain. Still, Bourguignon *et al.* verified that β-lapachone reduced the activity (>65%) of *T. cruzi* proteic whole extract of cysteine proteinase at 4.9 ± 1.0 μmol min^{-1} mg of $protein^{-1}$ concentration. Zani *et al.*[7] and Zani & Fairlamb[46] identified that compound **(1)** (Figure 2) presents a non-competitive inhibition mode upon the recombinant trypanothione reductase (TR) from *T. cruzi*. Besides, it was able to reduce the growth of epimastigotes. According to a study performed by Jorqueira *et al.*,[47] it was found that an oxyrane derivative of α-lapachone **(2)** (Figure 2) has activity against epimastigote of *T. cruzi* Dm28C strain. Considering the previously reported results for β-lapachone, Ferreira *et al.*[48] performed a study that identified the compound **(3)** as a trypanocidal agent against trypomastigotes of *T. cruzi*. Recently, Klein *et al.*[18] developed naphthoquinones containing a dipeptide sequence H_2N-L-Phe-L-Leu-OBn attached in their *N*-terminal regions since RhD to hydrolyze compounds with this recognition unit. Then, the authors identified analog **(4)** as a potent, time-dependent, and reversible inhibitor of RhD.

Herein, we performed a virtual screening of a small *in-house* library of 120 natural and nature-based compounds upon CRZ and RhD to identify promising cysteine protease inhibitors. Fourteen 1,4-naphthoquinone-based compounds were found to be potentially active toward these targets. Subsequently, these molecules were synthesized and

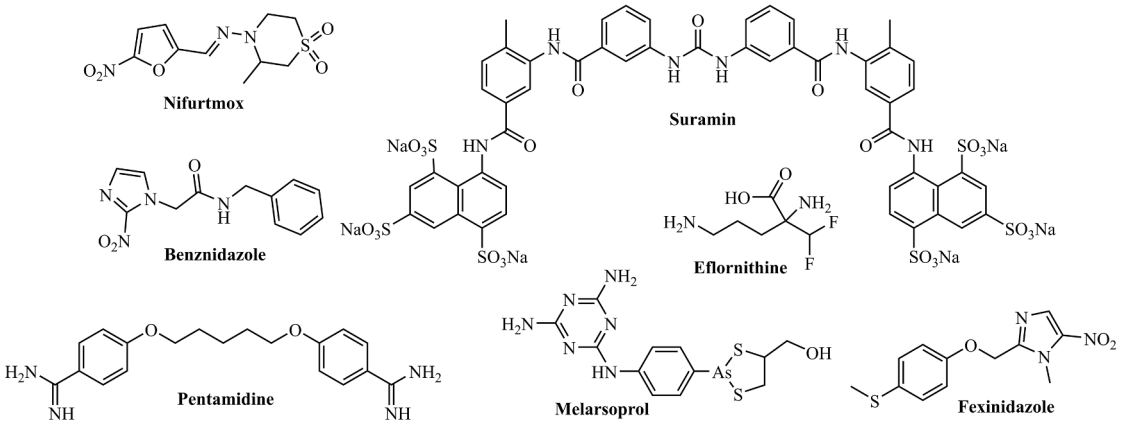

Fig. 1. Therapeutic arsenal used in the treatment of Chagas disease and Human African Trypanosomiasis (HAT).

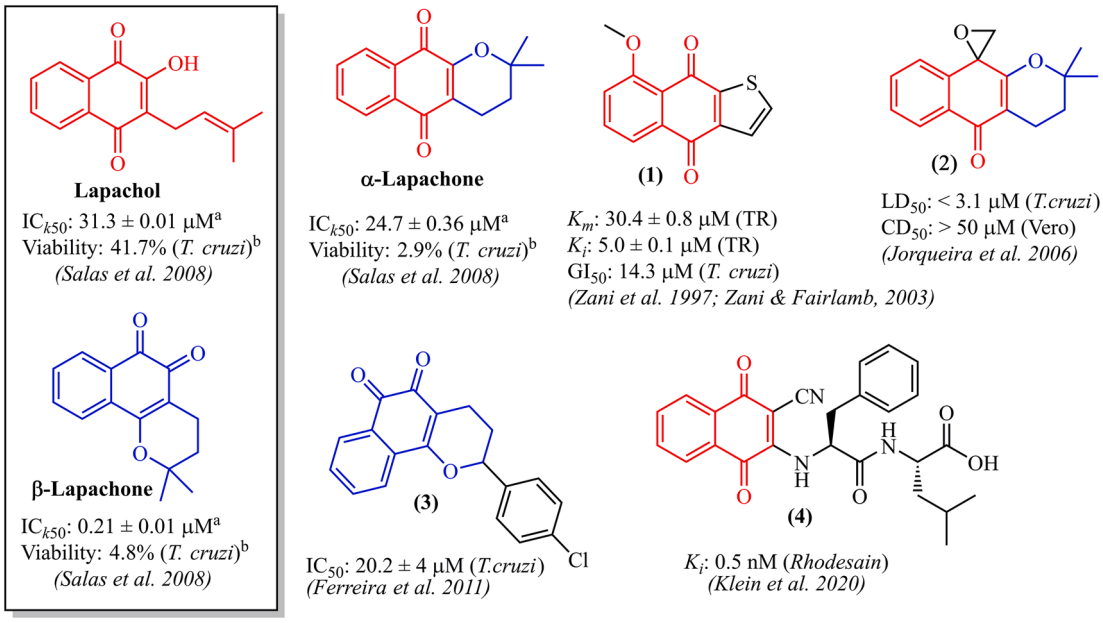

Fig. 2. Lapachol- and *β*-Lapachone-based compounds with trypanocidal activity. *TR*: trypanothione reductase; k_m: *Michaelis constant;* k_i: *inhibitory constant;* GI_{50}: *growth inhibition for 50%;* [a]: *concentration needed to decrease the growth constant* (k_c) *by 50%;* [b]: *viability of infected Vero cells with trypomastigote of T. cruzi.*

screened for their inhibitory activities. After structure–activity relationship (SAR) analyses, compound **JN-11** was identified as a hit compound in this study as a time-dependent inhibitor. Posteriorly, molecular docking and dynamic simulations were performed to obtain data on its interactions and complex stability, respectively. Furthermore, all dynamics' trajectories were used to perform MM-PBSA calculations to obtain essential physicochemical parameters on CRZ- and RhD-**JN-11** complexes. Subsequently, we hypothesized a possible covalent mechanism of inhibition for **JN-11**, which was investigated by covalent molecular docking and Density Functional Theory (DFT) calculations at an atomistic level. Figure 3 summarizes the workflow followed for this study. Further analyzes involving reversibility by dilution assays were performed to evaluate our hypothesis. All methods and results described in this study can be useful for other research teams worldwide,

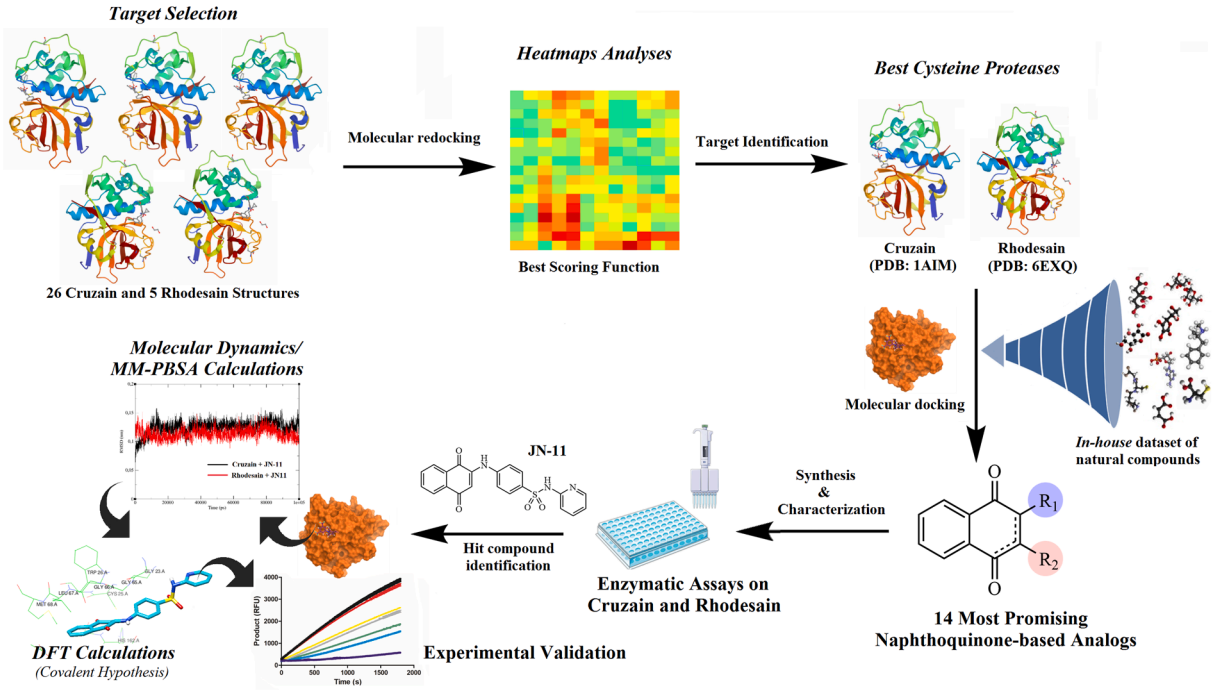

Fig. 3. Rational design and study overview employed to identify 1,4-naphthoquinone-based compounds as inhibitors of cruzain and rhodesain cysteine proteases. *Initially, a dataset of cysteine proteases (CRZ and RhD) was used to perform molecular redocking simulations to identify the most accurate scoring function, validated by heatmaps. Subsequently, the most accurate algorithm was used to virtually screening a small group of 120 in-house natural and nature-based compounds. Then, substituted naphthoquinone-based compounds were identified as promising inhibitors, which were posteriorly synthesized and biologically evaluated against CRZ and RhD enzymes. Finally, the hit compound was identified and explored by molecular dynamics (MM-PBSA), DFT calculations, time-dependence inhibition and reversibility assays to investigate a possible covalent mechanism of inhibition.*

increasing the chances to obtain promising drug candidates in the future.

2. Results and discussion

2.1. Virtual Screening, Identification, and synthesis of Naphthoquinone-based compounds

In our virtual screening protocol, 26 CRZ and 5 RhD structures complexed with inhibitors were obtained from the PDB website. Subsequently, molecular redocking simulations were performed using four scoring functions, ChemPLP, GoldScore, ChemScore, and ASP, from the GOLD® software. Thus, RMSD values were found ranging from 0.238 to 4.839 Å for CRZ, while from 0.383 to 3.105 Å for RhD (see Supplementary Material, Table S1 and S2). Regarding redocking solutions, RMSD values allow to categorize them as: (*i*) good solutions when RMSD values are less than 2.0 Å; (*ii*) acceptable solutions when RMSD values ranging from 2.0 to 3.0 Å; and (*iii*) bad solutions when RMSD values are higher than 3.0 Å.[49–52] ChemPLP showed the most accurate scoring function for both cysteine proteases, presenting the lowest RMSD values in redocking simulations. Additionally, the ChemPLP algorithm estimated FitScore values of 50.03 and 52.74 toward CRZ and RhD, respectively.

CRZ and RhD structures (PDB id 1AIM[53] and 6EXQ,[54] respectively) were selected based on their RMSD values. Posteriorly, a small *in-house* dataset of 120 natural and nature-based compounds was investigated for their potential activity upon CRZ and RhD. Among these compounds, fourteen 1,4-naphthoquinone analogs (with FitScore values $\geq$ 53, see Supplementary Material, Figure S1), including **lapachol**, were identified as promising inhibitors for both proteases. Then, some of them were purchased, and others were synthesized. **Lapachol** was obtained from extracts of *Tabebuia* sp. bark, with 1–2% yield. In general, all compounds were obtained by nucleophilic attack of the most basic nitrogenated reagents directly into the carbonyl group (C1-addition) or in the carbon from the 1,4-naphthoquinone core (*C*2-addition),[55] with yields ranging from 39 to 95%. Scheme 1 shows all compounds obtained in this study, including their synthetic routes and reaction conditions. Finally, all these compounds were evaluated in enzymatic assays against CRZ and RhD proteases. These results will be discussed in the next section.

Fourier transform infrared spectroscopy (FTIR) data were used to identify the major functional groups present in this series of compounds. In general, FTIR spectra of products showed the deformation bands (δ) of OH and NH groups in 3485–3305 cm^{-1} regions. Moreover, bands of stretching vibrations (ν) for carbonyl groups ($_{\nu}C=O$) were found from 1678 to 1591 cm^{-1} region, while ($_{\nu}C=S$) was observed at 1678 cm^{-1} for **AS12/15**. Still, ($_{\nu}C–N$) vibration ranged from 1265 to 1140 cm^{-1} region, while ($_{\nu}C–O$) at 1043 cm^{-1} for **JN-17**. Furthermore, stretching vibrations for SO_2 groups were observed at 1142 and 1167 cm^{-1} for **JN-11** and **JN-13**, respectively. ^1H NMR spectra of the compounds exhibited chemical shifts (δ) concerning the aromatic hydrogens from the naphthalene ring, ranging from δ 7.8 to 8.6 ppm as doublets and triplets. The singlet corresponding to the hydrogen CH (C3) from the naphthalene ring was observed from δ 5.4 to 6.4 ppm. Considering the isonicotinoylhydrazide substituent present at **IK-01**, **JN-22**, and **CR-70**, the four pyridyl protons were assigned ranging from δ 7.8 to 8.9 ppm. For **AS12/15**, **IK-01**, **JN-22**, and **CR-70**, the singlet for the NH group was displayed in the range of δ 8.1 and 11.0 ppm. The presence of the NH peak great than 10.0 ppm was indicative of conformation in which there is a hydrogen bonded to the carbonyl oxygen (C═O).[55] Also, this fact was proved by DFT calculations (see Supplementary Material, Figure S2), using **JN-22** as example. The presence of a largely deshielded signal in the range of δ 14.9 to 16.4 ppm in hydrazone analogs **AS-12/**

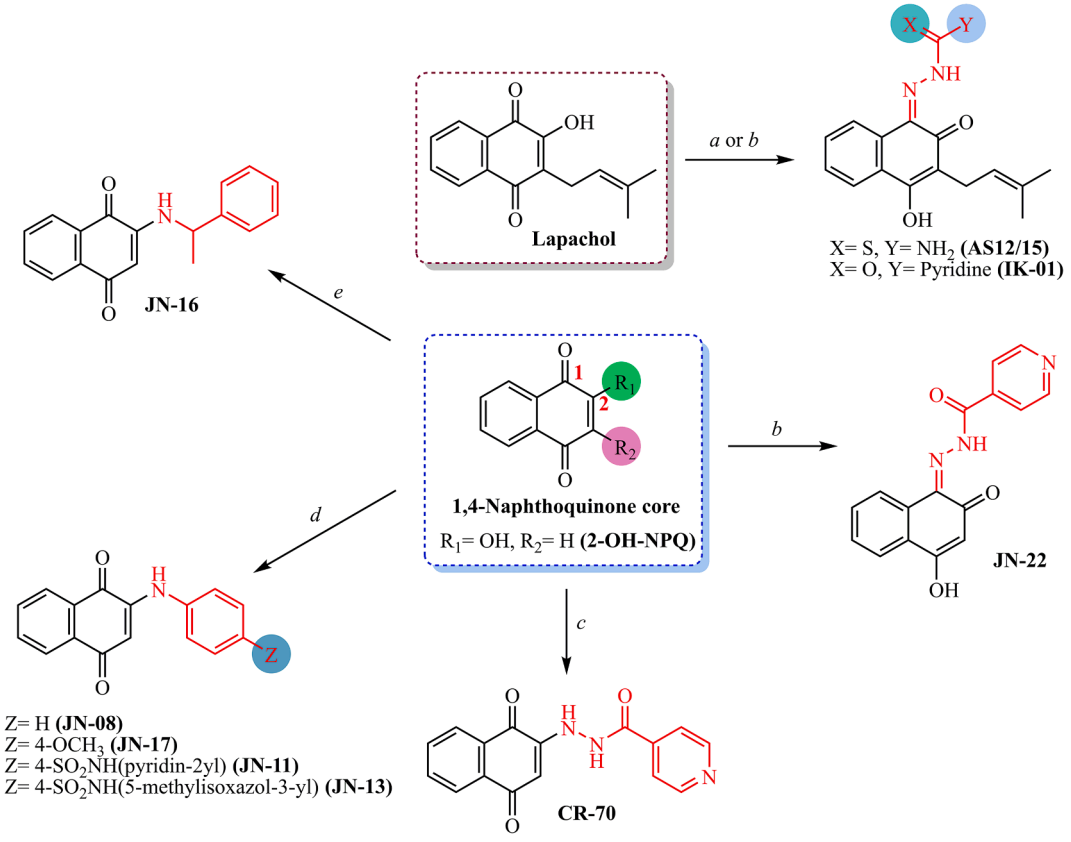

Scheme 1. Synthetic routes to obtain naphthoquinone-based compounds. *Reaction conditions: (a) step 1- NaOH 0.1 M, thiosemicarbazide methanolic solution; step 2- HCl 10% solution. (b) Et_3N 10% solution, isonicotinoyl hydrazide, acetic acid glacial. (c) Acetic acid glacial 80% solution, isonicotinoylhdrazide aqueous solution. (d) H_2O or EtOH, aromatic amine. (e) N-methylbenzylamine, DMF, 80 °C.*

15, **IK-01**, and **JN-22** was indicative of *Z*-conformation established by the intramolecular NH···O═C six-membered hydrogen bonded ring.[55] In addition, our analysis of (*Z*)-stereochemistry for the C═N imine double bond in acylhydrazones derivatives (**IK-01** and **JN-22**) or the thiosemicarbazone (**AS12/15**) is corroborated by the results presented by Campos *et al.*[56] In this work, the authors defined the stereochemistry based on their analysis of ^{1}H NMR spectra and X-ray crystallographic data. ^{13}C NMR spectra for these naphthoquinone derivatives revealed the carbonyl groups (C═O) ranging from δ 179.7 to 184.6 ppm, suggesting that the 1,4-naphthoquinone core was preserved and substitutions with nitrogenated substituents occurred at the *C*2 carbon (**JN-16**, **JN-11**, **JN-13**, and **CR-70**). Aromatic carbon signals (C_{Ar}) for all analogs were recorded in the range of δ 122.1–134.8 ppm. Finally, signals for C = NNH groups from **IK to 01** and **JN-22** were observed varying from δ 127.5 to 129.5 ppm. Still, chemical shifts for C═O from the acylhydrazone group were computed from δ 155.5 to 170.3 ppm for these compounds. C═S peak from **AS12/15** was observed at δ 179.5 ppm. HPLC analyzes revealed that these compounds present retention time (R_T) values ranging from 2.88 to 5.35 min, with purities varying from 95.0 to 99.9%. Finally, all chemical data are in agreement with the literature.[55,57]

2.2. Enzymatic activity on cruzain and rhodesain

All 1,4-naphthoquinone-based analogs were evaluated for their inhibitory activity toward CRZ and RhD enzymes, following the protocol described in the Material and Methods section. Results are presented in Table 1. Compounds **AS12/15**, **IK-01**, and **JN-11** were the most promising analogs against CRZ, showing IC_{50} values of 34 ± 1, 33 ± 2, and 6.3 ± 0.1 μM, respectively. Regarding the anti-RhD activity, **2-OH-NPQ**, **lapachol**, **AS12/15**, **IK-01**, and **JN-11** were found to be the most active compounds, exhibiting IC_{50} values of 33 ± 7, 58 ± 3, 28 ± 1, 20 ± 1, and 1.8 ± 0.1 μM, respectively. Surprisingly, **lapachol** and **2-OH-NPQ** were selective for RhD since these analogs did not demonstrate activity against CRZ. In contrast, **AS12/15**, **IK-01**, and **JN-11** could be considered broad-spectrum inhibitors since these molecules inhibited both of these proteases. Finally, a complete discussion on chemical substituents and their influences on the activity is provided in the SAR analysis section. Compound **JN-17** displayed a very poor solubility at testing conditions, preventing the determination of its biological activity. In Figure 4 are shown IC_{50} curves for all active compounds against CRZ and RhD.

Table 1
Inhibitory activity of naphthoquinone-based compounds toward cruzain and rhodesain proteases.

Compound	% Cruzain inhibition (100 μM)[a]	IC_{50} cruzain (μM)[b]	% Rhodesain inhibition (100 μM)[a]	IC_{50} rhodesain (μM)[b]
2,3-Cl-NPQ	49.0 ± 3.0	ND	56.0 ± 4.0	ND
2-Br-NPQ	51.0 ± 2.0	ND	50.0 ± 2.0	ND
2-OH-NPQ	58.0 ± 2.0	ND	**77.0 ± 3.0**	**33.0 ± 7.0**
2-OCH_3-NPQ	32.0 ± 4.0	ND	27.0 ± 0.0	ND
Lapachol	35.0 ± 2.0	ND	**70.0 ± 7.0**	**58.0 ± 3.0**
AS12/15	**83.0 ± 1.0**	**34.0 ± 1.0**	**82.0 ± 2.0**	**28.0 ± 1.0**
IK-01	**76.0 ± 2.0**	**33.0 ± 2.0**	**87.0 ± 2.0**	**20.0 ± 1.0**
JN-08	48.0 ± 3.0	ND	61.0 ± 2.0	ND
JN-11	**95.0 ± 1.0**	**6.3 ± 0.1**	**93.0 ± 0.0**	**1.8 ± 0.1**
JN-13	6.0 ± 2.0	ND	1.0 ± 1.0	ND
JN-16	26.0 ± 2.0	ND	23.0 ± 3.0	ND
JN-17	NT	NT	NT	NT
JN-22	66.0 ± 5.0	ND	52.0 ± 2.0	ND
CR-70	37.0 ± 2.0	ND	37.0 ± 2.0	ND
E-64 (2 μM)	99.0 ± 1.0	0.02 ± 0.1	99.0 ± 2.0	0.0031 ± 0.0

[a] Results represent the average and standard error of two independent experiments in triplicate. Errors are given by the ratio between the standard deviation and the square root of the number of measurements. [b]: IC_{50} values represent the average of two independent experiments determined based on at least 8 compound concentrations in triplicate. Errors are given by the ratio between the standard deviation and the square root of the number of measurements. ND: Not determined. NT: Not tested.

2.3. Structure-Activity relationship (SAR) analysis

Regarding the biological results obtained from the enzymatic assays performed on CRZ and RhD presented in Table 1, SAR analysis was performed to identify the most promising molecular features found in this small series of 1,4-naphthoquinone-based compounds. Initially, **lapachol** was assumed as the starting point for such analysis. Subsequently, electron-withdrawing and electron-donating groups at position 2 were analyzed, followed by substituted aniline, isonicotinoylhydrazide, thiosemicarbazone, and sulfonyl groups, at positions 1 or 2. Furthermore, the inhibition results for those compounds on CRZ at 100 μM concentration will be first discussed, and then RhD results.

Initially, screening was performed at 100 μM, **lapachol** displayed low activity upon CRZ, with 35 ± 2% inhibition. However, when two electron-withdrawing atoms, such as chlorine atoms, are inserted at positions 2 and 3 from the 1,4-naphthoquinone core (**2,3-Cl-NPQ**), the activity is slightly increased, showing 49 ± 3% inhibition. This activity is still increased when a bromine atom is present at position 2 (and position 3 remains unsubstituted), a compound with 51 ± 2% inhibition is obtained (**2-Br-NPQ**). When this bromine atom is replaced with a strong electron-donating group (**2-OH-NPQ**), the enzymatic activity is improved, exhibiting 58 ± 2% inhibition.

When it is substituted with a methoxyl group (**2-OCH_3-NPQ**), a reduction in the activity is about 1.8-fold. Concerning nitrogenated substituents, it is verified that a 1-phenylethylamino group at position 2 (**JN-16**) significantly reduces the activity on CRZ, showing only 26 ± 2% inhibition. In contrast, the replacement of this group with an aniline ring generates a compound more active (**JN-08**), which demonstrates 48 ± 3% inhibition at 100 μM concentration. Unfortunately, when this aniline ring is substituted at *para*-position with a methoxyl group, a compound (**JN-17**) with poor solubility is obtained since it was impossible to test it. Then, introducing an isonicotinoylhydrazide at position 2 (**CR-70**), a compound less active than **JN-08** is provided, exhibiting 37 ± 2% inhibition. Considering **JN-08**, when a sulfonamide-isoxazole group is inserted at the *para*-position, the most poorly active compound is obtained (**JN-13**), exhibiting only 6 ± 2% inhibition. In contrast, when the isoxazole ring is replaced with a 2-pyridine ring, the best compound of this series (**JN-11**) was generated, exhibiting 95 ± 1% inhibition, resulting in an IC_{50} value of 6.3 ± 0.1 μM. Considering **lapachol** structure, when the isonicotinoylhydrazide group is placed at position 1 (**IK-01**), its enzymatic activity is significantly improved, exhibiting 76 ± 2% inhibition, with an IC_{50} value of 33 ± 2 μM. Surprisingly, when the isoprene unit at position 3 is removed is observed a slight reduction in the activity, generating **JN-22** with 66 ± 5% inhibition. Regarding **IK-01**, when the nitrogenated group at position 1 is replaced with a thiosemicarbazone substituent, an even more active compound is obtained (**AS12/15**), displaying 83 ± 1% inhibition, resulting in an IC_{50} value of 34 ± 1 μM.

Regarding the RhD inhibition, it was observed that **lapachol** was more active upon RhD than CRZ, exhibiting 70 ± 7% inhibition, which resulted in an IC_{50} value of 58 ± 3 μM. Compounds **2,3-Cl-NPQ** and **2-Br-NPQ** demonstrated equivalent active profiles, with inhibition values of 56 ± 4 and 50 ± 2%, respectively. It suggests that there are no meaningful differences between these weak electron-withdrawing groups. The strong electron-donating group, such as the hydroxyl substituent from the **2-OH-NPQ**, improves the activity upon RhD than **2-OCH_3-NPQ**. It demonstrated 77 ± 3% inhibition, resulting in an IC_{50} value of 33 ± 7 μM, while **2-OCH_3-NPQ** presented only 27 ± 0% inhibition. Concerning the aminated substituents, **JN-16** displayed a similar

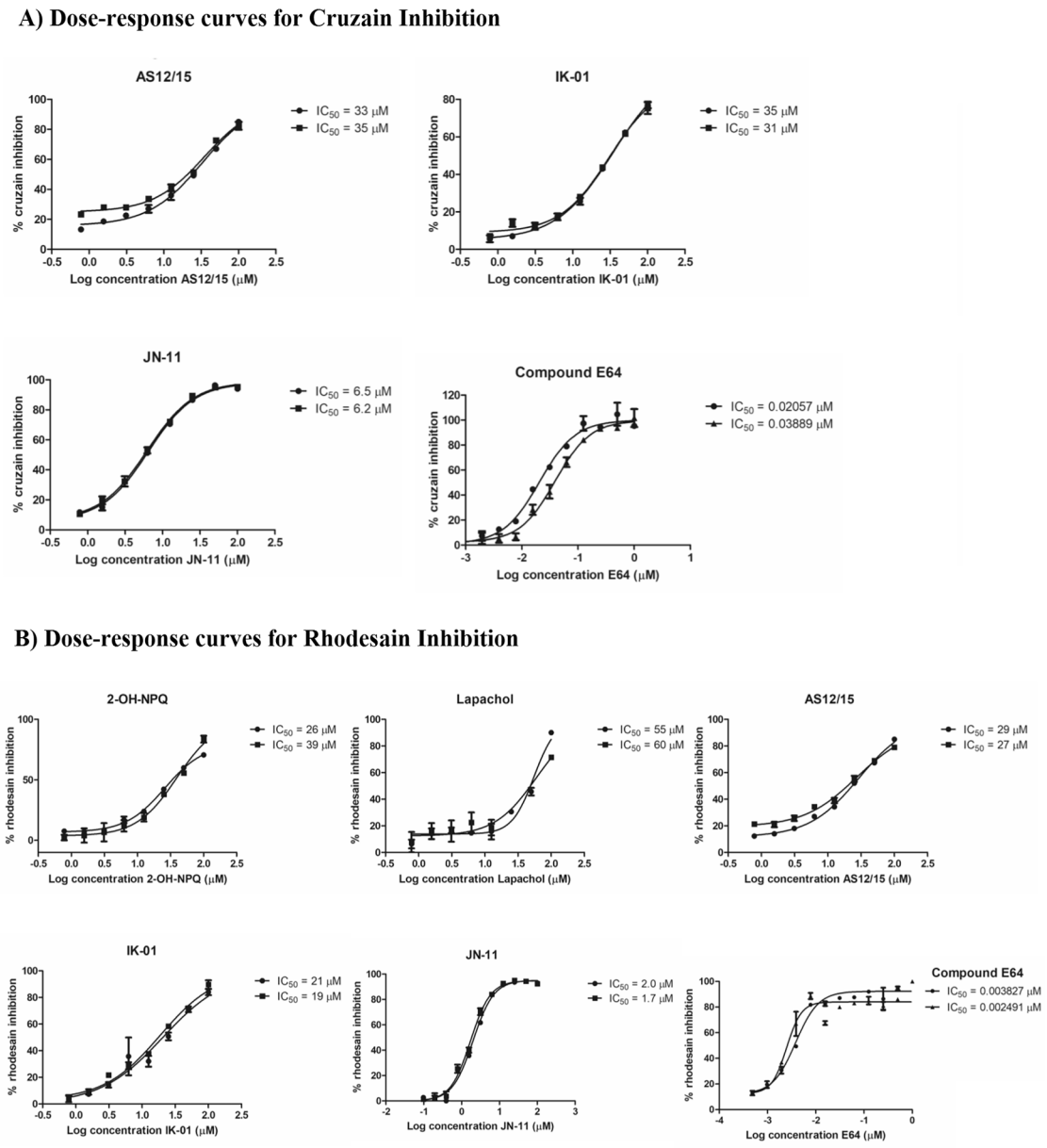

Fig. 4. Dose-response curves for cruzain and rhodesain inhibition. *In A, Dose-response curves for cruzain compounds **AS12/15**, **IK-01**, and **E64**. In B, Dose-response curves for rhodesain inhibition compounds **2-OH-NPQ**, **Lapachol**, **AS12/15**, **IK-01**, and **E64**. IC_{50} curves represent two independent experiments, which were determined using at least eight different concentrations of the compounds in triplicate.*

inhibition profile for CRZ and RhD, showing 23 ± 3% inhibition. Moreover, the 1-phenylethylamino group at position 2 reduces the activity towards RhD in comparison with **2-OCH$_3$-NPQ**. When this substituent is replaced with an aniline ring (**JN-08**) occurs a modest increase in the activity. In contrast, when this new group has a sulfonamide coupled to an isoxazole ring at the *para*-position results in the inactivation of the analog (**JN-13**) since it presented 1 ± 1% inhibition. When the isoxazole ring is replaced with a 2-pyridine ring, the most active compound is obtained (**JN-11**), displaying 93 ± 0% inhibition, which resulted in an IC_{50} value of 1.8 ± 0.1 μM. Like against CRZ, it was found to be the hit compound towards RhD. Additionally, when this chemical group at position 2 is replaced with an isonicotinoylhydrazide (**CR-70**) is observed a significant reduction in its activity, showing only 37 ± 2% inhibition. When the **lapachol** structure is modified at position 1, introducing an isonicotinoylhydrazide group (**IK-01**), is observed a significant increase in the activity, resulting in 87 ± 2% inhibition and an IC_{50} value of 20 ± 1 μM. Still, when this group is replaced with a thiosemicarbazone group, a compound with similar effects is obtained (**AS12/15**), with inhibition and IC_{50} values of 82 ± 2% and 28 ± 1 μM, respectively. However, when the isonicotinoylhydrazide group remains at the same position and the isoprene unit is removed from position 3, it is observed a meaningful reduction in the activity (**JN-22**), exhibiting 52 ± 2% inhibition. Finally, we would like to clarify that all SAR discussions focused on compounds with demonstrating only %inhibition values were performed considering observations only at 100 μM concentration, obtained by two independent experiments in triplicates, we did not consider trends in different concentrations in this SAR discussion.

2.4. Molecular docking simulations on cruzain and rhodesain

As described in the previous section, initially, we discussed CRZ results and then RhD. For all compounds, their interactions can be found in the Supplementary Material (Figures S3-S15). Additionally, none of

these 1,4-naphthoquinone compounds interacted with the complete catalytic triad from both cysteine proteases. Among the interactions observed from CRZ-naphthoquinone complexes, van der Waals, π-sulfur, and π-alkyl interactions are frequently displayed, in which the most frequent amino acid residues are Gly[66], Met[68], and Ala[133]. In general, these 1,4-naphthoquinone analogs interact with several amino acids from the CRZ binding site, in which the number of amino acids involved ranges from 11 to 18 residues, being **AS12/15** and **IK-01** compounds with the highest number of residues involved in their complexes' formation. Moreover, it was verified that Cys[25], Trp[26], Gly[66], Leu[67], Met[68], Ala[133], Leu[157], Asp[158], and Glu[205] residues are present in all ligands' interactions. All of these compose a pocket surrounding these analogs on CRZ (Figure 5A). Then, these amino acids could be considered as characteristics for this chemotype of natural and nature-based compounds. According to Bourguignon *et al.*,[58] this chemical class of compounds is typically placed into the CRZ S2 pocket, interacting with Ser[64], Gly[66], Leu[67], Met[68], Ala[133], Leu[157], Gly[160], and Glu[205], corroborating with our results. For CRZ, all compounds are capable of interacting with Cys[25] and His[159] residues, except for **JN-08**, which interacts only with Cys[25]. The best CRZ inhibitors (**AS12/15**, **IK-01**, and **JN-11**) presented interactions involving 18, 18, and 14 amino acid residues, respectively. These analogs have exclusive interactions with some residues, being Gln[19] for **AS12/15**, Asp[60] and Val[134] for **IK-01**, and Gln[115] for **JN-11**, in which were observed van der Waals interactions between them. It suggests that these amino acid residues could be associated with a significant role in the CRZ inhibition by 1,4-naphthoquinone-based analogs.

Regarding the results of molecular docking toward RhD (see Supplementary Material, Figure S15-S28), it was verified that these compounds present several interactions varying from 12 (for **2,3-Cl-NPQ** and **2-Br-NPQ**) to 17 (for **lapachol** and **IK-01**) residues. However, the most active compounds on RhD (**2-OH-NPQ**, **JN-11**, **AS12/15**, **IK-01**, and **lapachol**) also present interactions involving 15–17 residues. All compounds interact with Cys[25], Trp[26], Gly[66], Leu[67], Met[68], Ala[138], Leu[160], and His[162] amino acid residues. All of these compose a pocket surrounding these analogs on RhD (Figure 5B). Additionally, it was observed that the most frequent chemical forces present in their complexes are van der Waals, hydrogen bonding, and π-alkyl interactions. Also, it was observed that none of these analogs are able to interact with the complete catalytic triad since it was verified all of them interact only with Cys[25] and His[162] residues. Surprisingly, among the most active compounds, three of them present exclusive interactions. For **AS12/15**, a sulfur-x interaction between its double bond (*C2* = C3) from the 1,4-naphthoquinone core and the sulfur atom at the Met[68] are present. For **IK-01**, a π-σ interaction was seen involving its 4-pyridine ring and a C—C sigma bond from the Ala[138] residue. For **lapachol**, it was observed a π-donor hydrogen-bonding interaction involving the carbonyl at C4 and Gly[163], and benzene ring and Gly[66] residue. Furthermore, only three molecules present interactions with exclusive residues, Phe[72] and Leu[204] for **IK-01**, Asp[117] for **JN-08**, and Ser[24] and Val[139] for **lapachol**. Lastly, these docking studies revealed that active 1,4-naphthoquinone-based compounds frequently interact with Cys[25], Trp[26], Gly[66], Leu[67], Met[68], Ala[138], Leu[160], Asp[161], His[162], and Gly[163] residues, corroborating with other previous studies.[58,59]

2.5. Molecular dynamics simulation on cruzain and rhodesain complexed with *JN-11*

Initially, the stereochemical quality of the most stable poses of dynamic simulations for CRZ and RhD structures was analyzed using the Ramachandran plot (see Supplementary Material, Figure S29 A and B). For CRZ, 88% of residues are found in favored regions, 11.5% in allowed regions; 0.5% in generously allowed regions; and 0.0% in not allowed regions (outliers). For RhD, 82% of residues are found in favored regions; 16.1% in allowed regions; 0.6% in generously allowed regions; and 0.6% in not allowed regions (outliers). Finally, these results are in accordance with reliable molecular models for performing virtual protocols.[60,61] Then, these optimized models in native form were used to explore the interactions of **JN-11** and both of these targets. Molecular dynamics evaluated the complexes' structural stability at trajectories of 100 ns. Thus, the results of C_α RMSD (Figure 6A) show average values ranging from 0.1 to 0.15 nm for both CRZ- and RhD-**JN-11** complexes. These complexes demonstrated to achieve the stabilization after 15 ns simulation, remaining stable during all the simulation time (100 ns). Still, it was verified that these complexes presented stable deviations (less than0.3 nm).[62] However, minor variations are observed for RhD-**JN-11** complex, suggesting high-stability for it. The RMSF plot (Figure 6B) revealed low fluctuations for the residues and even minor fluctuations for the catalytic triad. Thus, **JN-11** at the active site does not promote significant conformational changes in primary amino acid residues. Additionally, the R_g plot (Figure 6C) shows conformational changes varying from 1.62 to 1.63 nm, indicating high-rigidity and compactness of the protein structure.[63] Another crucial data to verify the complexes' stability was SASA analysis (Figure 6D). The results demonstrate that during the simulation time, the area accessible to the solvent did not present significant alterations, ranging from 93 to 103 nm^2, suggesting that **JN-11** does not modify the protein structure and it

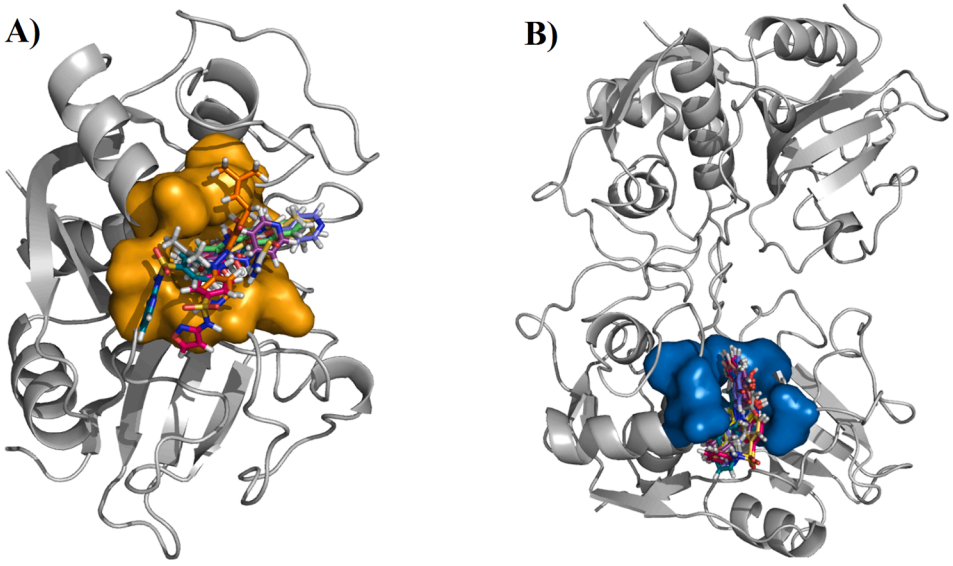

Fig. 5. Cluster of naphthoquinone derivatives into the binding site of cruzain (A) and rhodesain (B). PDB ids: 1AIM for cruzain and 6EXQ for rhodesain.

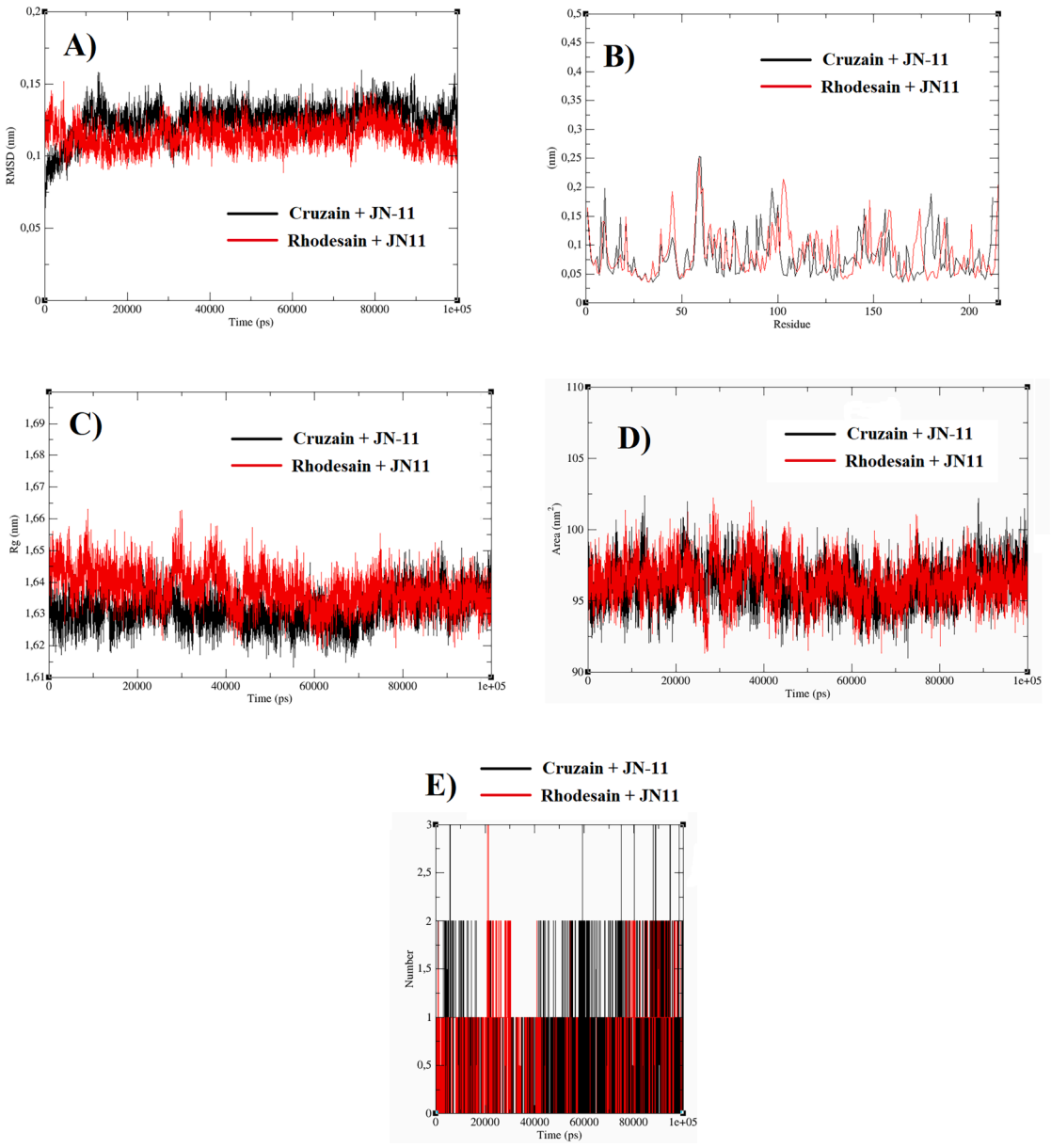

Fig. 6. Post-molecular dynamics analysis for 100 ns simulation time for cruzain (black line) and rhodesain (red line) complexed with JN-11. *In (A), C_α RMSD plot; (B): RMSF plot; (C): Radius of gyration (R_g). (D): Surface area solvent accessible (SASA). (E): Hydrogen-bonding interactions plot.*

remains at the active site. It should be considered that increased SASA values indicate greater exposure of the ligand to the environment exposed to the solvent.[64] Figure 6E shows that **JN-11** performs up to three hydrogen-bonding interactions during the simulation time, suggesting that these could be stabilizing forces for these complexes. These results revealed excellent complexes' stabilities, which may indicate the best activity observed for **JN-11** against both CRZ and RhD.

Evaluation of interactions post-dynamic simulations analysis for **JN-11** was performed to check if CRZ and RhD active sites are altered by introducing chemical paramters. **JN-11** showed similar interactions for both proteases, such as π-alkyl with Leu[67], Ala[138], and Leu[160]; π-sulfur with Cys[25] and Met[68], and van der Waals with Trp[26], Gly[65], Gly[66], and His[159/162] residues. On the other hand, **JN-11** performed two hydrogen-bonding interactions with Gly[23] (3.47 Å) and Gly[163] (3.08 Å) residues (Figure 7A) at the CRZ active site, while three hydrogen-bonding interactions were observed for RhD, involving Gly[23] (3.93 Å), Cys[63] (2.06 Å), and Gly[163] (3.75 Å) residues (Figure 7B). In general, these interactions are associated with the inhibition of these targets. Finally, we believe that the most significant activity of **JN-11** towards RhD is possibly associated with its H-bonds performed at the active site.

2.6. *MM-PBSA calculations for **JN-11** in complex with cruzain and rhodesain*

Using trajectories from dynamic simulations, the determination of free binding energy ($\Delta G_{binding}$) values was done by MM-PBSA calculations (Table 2), performing a re-score of **JN-11** and characterizing its main interactions. As expected, **JN-11** exhibited high-affinity for RhD active site ($\Delta G_{binding}$ = -25.3 ± 3 Kcal mol^{-1} ± SD) than for CRZ active site ($\Delta G_{binding}$ = -12.6 ± 4 Kcal mol^{-1} ± SD), corroborating with our experimental results. Moreover, MM-PBSA calculations revealed that van der Waals interactions are the main forces involved in the coupling process for both proteases, with favorable energy values for CRZ (-21.7 ± 5.2 Kcal mol^{-1} ± SD) and RhD (-40.3 ± 2.3 Kcal mol^{-1} ± SD) when compared to electrostatic forces for CRZ and RhD (-2.7 ± 2.7 and −4.8 ± 2.2 Kcal mol^{-1} ± SD, respectively). Interestingly, RhD-**JN-11** complex

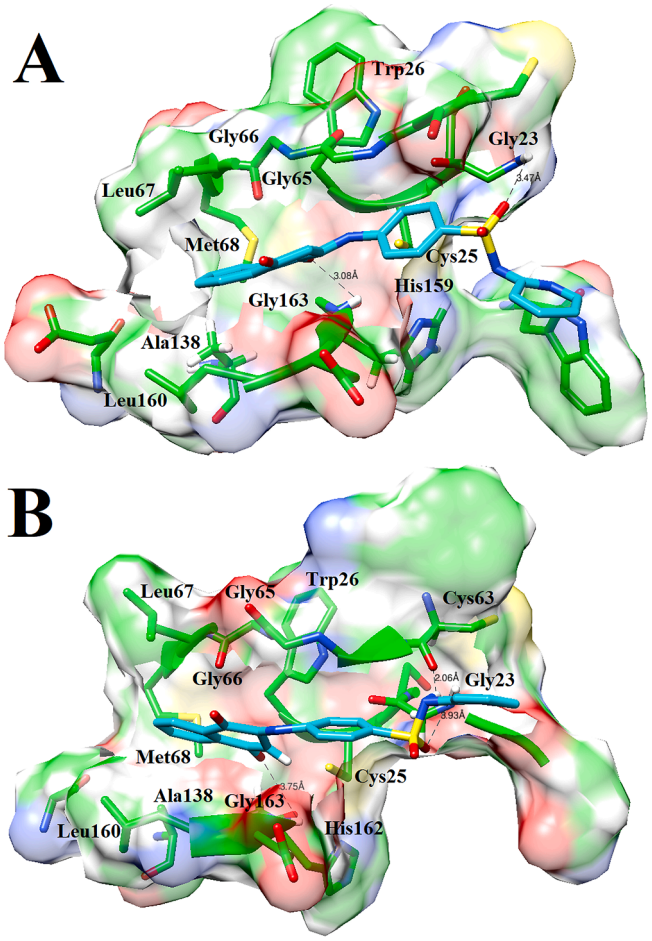

Fig. 7. Molecular interactions for JN-11 in complex with cruzain (A) and rhodesain (B) after dynamic simulations at 100 ns.

Table 2
Binding energy from cruzain- and rhodesain-JN-11 complexes estimated by MM-PBSA calculations.

Parameters	Complex (Kcal mol^{-1} ± SD) CRZ-JN-11	RhD-JN-11
Binding Energy ($\Delta G_{binding}$)	$^{-1}$2.6 ± 4.0	−25.3 ± 3.0
SASA Energy	−2.5 ± 0.4	−3.7 ± 0.2
Polar Solvation Energy	14.4 ± 5.5	23.6 ± 2.9
Electrostatic Energy	−2.7 ± 2.7	−4.8 ± 2.2
Van der Waals Energy	−21.7 ± 5.2	−40.3 ± 2.3

presented lower SASA energy values (-3.7 ± 0.2 Kcal mol^{-1} ± SD), suggesting that **JN-11** is placed into a hydrophobic environment at the RhD active site, with less exposure to water molecules from the physiological medium, when compared with CRZ active site (-2.5 ± 0.4 Kcal mol^{-1} ± SD). Finally, higher values of polar solvation energy for CRZ and RhD (14.4 ± 5.5 and 23.6 ± 2.9 Kcal mol^{-1} ± SD, respectively) indicate that the solvation of proteases is significant for both complex formations. Lastly, all these energetic data corroborate with the higher affinity of **JN-11** at the active site, corroborating with its IC_{50} value towards RhD.

It is known that the chemical reactivity of the 1,4-naphthoquinone nucleus is associated with its α,β-unsaturated system, which has an ambident behavior when reacting with nucleophiles, being able to undergo β-olefinic attack (1,4 addition) or direct addition to the carbonyl (1,2-addition). Thus, the preferred position of the addition will depend on the nature of the nucleophile and the reaction conditions.[55] Their chemical reactivities (via covalent mechanism) have been investigated in different studies.[18,36,65–67] Considering these data, we hypothesized that **JN-11** could be a potential covalent inhibitor and, then, we decided to investigate our hypothesis by using covalent docking simulations and DFT calculations. Posteriorly, we performed experimental assays to verify our suppositions.

2.7. Our hypothesis of covalent inhibition for *JN-11*

2.7.1. Covalent molecular docking simulation

Using the most stable pose obtained from dynamic simulations at 100 ns, CRZ- and RhD-**JN-11** complexes were investigated for a possible covalent mechanism of inhibition. Then, covalent docking simulations were used to predict if **JN-11** could undergo a nucleophilic attack by $Cys^{25}(S^-)$ residue (also, named as thiolate anion) at the C3 atom from the 1,4-naphthoquinone core since this nucleophilic residue was located at distances of 5.72 and 3.92 Å for CRZ and RhD, respectively. Romeiro *et al.* suggested that these distance values should be lower than 4.65 Å to result in a potential covalent inhibiton.[68] It was observed that **JN-11** exhibits a higher covalent score value for C3-Michael-addition by RhD (9.78) than for CRZ value (6.05), suggesting that a higher probability of **JN-11** to be attacked by the thiolate anion from RhD protease. These results may be associated with distances between the C3 atom and Cys^{25} residue. Additionally, *C*2-Michael-additions were also explored toward both enzymes. Nevertheless, low covalent score values were obtained (below 4.05) for both proteases. Recently, studies involving broadly employed docking software concluded that none of them is capable of predicting accurate Gibbs free energy values for covalent interactions (ΔG) and their rate-limiting barriers of transition states ($\Delta G^{\ddagger}$).[69–72] In contrast, quantum mechanics (QM) can be used for modeling biological systems due to its ability to describe chemical systems with quantitatively accurate values of ΔG and $\Delta G^{\ddagger}$.[73–75] Notwithstanding these data, it was decided to investigate a mechanistic hypothesis involving C3-Michael-addition of **JN-11** towards RhD, employing quantum chemistry calculations by DFT.

2.7.2. Atomistic covalent mechanism for *JN-11* by DFT calculations

In the literature is reported that the catalytic mechanism of cysteine proteases depends on two residues at the active site, which typically is composed of Cys and His amino acids. Besides, it is known that the physiological environment favors that the imidazole group from the His residue polarizes the SH group from the Cys residue, leading to the highly nucleophilic $Cys(S^-)/His(H^+)$ ion pair.[76–79] This ion pair is responsible for the high reactivity of these proteases toward electrophilic groups, broadly used in the development of covalent inhibitors.[76–79] Based on these facts, Density Functional Theory (DFT) calculations at the 6–31 + G* basis set were employed to predict the formation of a covalent complex involving **JN-11** and RhD, describing $\Delta G^{\ddagger}$ and ΔG values.

According to our hypothesis, **JN-11** has a Michael-acceptor system that could undergo a nucleophilic addition or substitution reaction at one of the carbon atoms from the α,β-unsaturated carbonyl group towards the cysteine residue at the active site of RhD.[18] In this context, we generated the intrinsic reaction coordinate (IRC) for our hypothesis, which revealed that the S^1 atom from Cys^{25} residue (at a distance of 3.95 Å) could attack the C3 atom from **JN-11**, via a Michael-addition mechanism (**JN-11-IC**) (Figure 8). Subsequently, S^1—C^3 connection results in an electron transfer from C3 = *C*2 bond to the oxygen atom (O^1) at C1, providing an oxy-anion (σ-complex) as a TS structure with a $\Delta G^{\ddagger}$ value of 7.78 kcal mol^{-1} (**JN-11-TS**). This increased resonance effect is responsible for reducing the bond lengths for C3 − *C*2 − C1 bonds from 1.42 to 1.40 Å for C3 − *C*2 bond, and from 1.44 to 1.42 Å for *C*2 − C1 bond. It was observed that there is an approximation of $Cys^{25}(S^1)$ to the C3 atom (1.77 Å) to perform a covalent bond. Additionally, it was verified that His^{162} residue has an essential role in stabilizing the TS geometry since it performs three hydrogen-bonding interactions at distances of 1.95, 2.19, and 1.63 Å for $H^1\cdots O^3$ − Cys, $H^2\cdots O^2$ − **JN-11**,

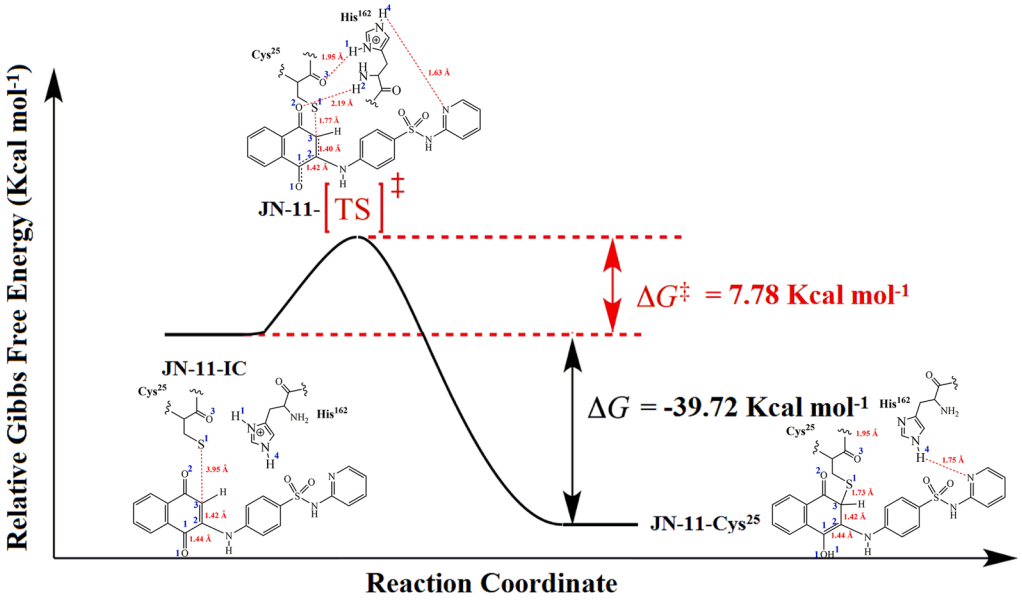

Fig. 8. Intrinsic reaction coordinate (IRC) displaying relative Gibbs free energy values for the nucleophilic attack of Cys^{25} residue at the C3 atom from compound JN-11. JN-11-IC: JN-11′s initial coordinates; JN-11-TS: JN-11′s transition state; JN-11-Cys^{25}: JN-11′s complexed with Cys^{25} residue (product).

and $H^4\cdots N^1$ − **JN-11**, respectively. Then, a stable product was obtained by regenerating the 1,4-naphthoquinone core, exhibiting a Δ*G* value of −39.72 Kcal mol^{-1} (**JN-11** − **Cys^{25}**). It was verified a covalent bond between Cys^{25}(S^1) and C3 atom from **JN-11**, with a bond length of 1.73 Å. Still, C3 − *C*2 and *C*2 − C1 bonds' lengths were again established, being 1.42 and 1.44 Å, respectively. Moreover, His^{162} residue performs only one hydrogen-bonding interaction with the final product via $H^4\cdots N^1$ − **JN-11**, at a distance of 1.75 Å. In general, this type of mechanism is assumed to occur in a two-stage one-step mechanism.[80] All these IRC results were supported by different studies found in the literature, which focused on nucleophilic substitutions of 1,4-naphthoquinones toward nucleophiles (including cysteine proteases), making our hypothesis more relevant. According to Delarmelina *et al.*,[36] sulfur-containing nucleophiles present TS values ranging from 4.7 to 5.06 Kcal mol^{-1} and, subsequently, their addition products exhibit Δ*G* values ranging from − 34.63 to − 38.91 Kcal mol^{-1}. Additionally, Arafet *et al.* developed studies involving cysteine proteases (falcipain-2 and CRZ) and QM/MM calculations,[76–78] which they verified that their catalytic mechanisms occur with TS values ranging from 10 to 29.5 Kcal mol^{-1}. Still, activation barriers (TS values) higher than 40 Kcal mol^{-1} were considered as unreasonable steps.[36,79] Valente *et al.* explored the mechanism of addition on C3-unsubstituted and *C*2-substituted naphthoquinone analogs and verified that this chemotype can undergo a nucleophilic attack at the C3-unsubstituted position.[81] Bruno *et al.* demonstrated also via kinetic and mass spectrometry studies that the glyceraldehyde-3-phosphate dehydrogenase from *T. brucei* (*Tb*GAPDH), a cysteine protease, can covalently bond to the C3-unsubstituted atom from a 1,4-naphthoquinone derivative, via a C3-Michael-addition mechanism of reaction.[82]

Even considering our IRC date presented here and all corroboration with the studies aforementioned, it was decided to investigate insights on this potential mechanism of inhibition by experimental analyzes performing time-dependence inhibition and reversibility assays, in order to evaluate our hypothesis. Furthermore, the hit compounds discovered in this study were also biologically evaluated.

2.7.3. Time-Dependence inhibition and reversibility assays

To gain more insights about the 1,4-naphthoquinone-based derivatives, we evaluated whether the five RhD hits were time-dependent inhibitors, a hallmark of covalent-acting molecules. Enzyme inhibition after 10 min pre-incubation with the compounds was compared to activity without preincubation.[83] RhD inhibition by compounds **2-OH-NPQ**, **Lapachol**, and **JN-11** was greater upon compound pre-incubation with the enzyme, consistent with a potential covalent mechanism of inhibition. In contrast, compounds **AS12/15** and **IK-01** did not show time-dependent inhibition. **AS12/15** and **IK-01** IC_{50} values were equivalent for both conditions, no pre-incubation and 10 min pre-incubation of these compounds with the target enzyme. In contrast, the time-dependent inhibitors (**2-OH-NPQ**, **Lapachol**, and **JN-11**) showed IC_{50} values, under no pre-incubation condition, higher than three times (Table 3).

A dilution experiment was performed to check whether the compounds were irreversible. We incubated the inhibitor and RhD at high concentrations and then diluting the incubation mixture to the apparent IC_{50} of the inhibitor.[83,84] Once this is done with RhD and E-64, a known irreversible cysteine protease inhibitor, the enzyme remained inhibited upon dilution, as expected. However, when the same test was carried out with the screening hits, full enzyme activity returned after dilution with compound **JN-11**. Most of the RhD activity was also observed in the presence of the other hits (Figure 9). This suggested that the inhibition by these hits is reversible.

Table 3
Time-dependence inhibition for the hit compounds.

Compound	%RhD inhibition (100 μM)[a]		IC_{50} RhD (μM)[b]	
	NI	I	NI	I
2-OH-NPQ	27.0 ± 1.0	77.0 ± 3.0	> 100	33.0 ± 7.0
Lapachol	18.0 ± 1.0	70.0 ± 7.0	> 100	58.0 ± 3.0
AS12/15	79.0 ± 2.0	82.0 ± 2.0	66.0 ± 3.0	28.0 ± 1.0
IK-01	73.0 ± 2.0	87.0 ± 2.0	29.0 ± 3.0	20.0 ± 1.0
JN-11	48.0 ± 2.0	93.0 ± 0.0	20.0 ± 3.0	1.8 ± 0.1
E-64 (0.1 μM)	7.0 ± 2.0	95.0 ± 1.0	N.D.	0.0031 ± 0.0

[a] : Results represent the average and standard error of two independent experiments in triplicate. Errors are given by the ration between the standard deviation and the square root of the number of measurements. [b]: IC_{50} values represent the average of two independent experiments which were determined based on at least 8 compound concentrations in triplicate. Errors are given by the ration between the standard deviation and the square root of the number of measurements. NI: Enzyme inhibition without pre-incubation with the compounds. I: Enzyme inhibition after 10 min pre-incubation with the compounds. ND: Not determined.

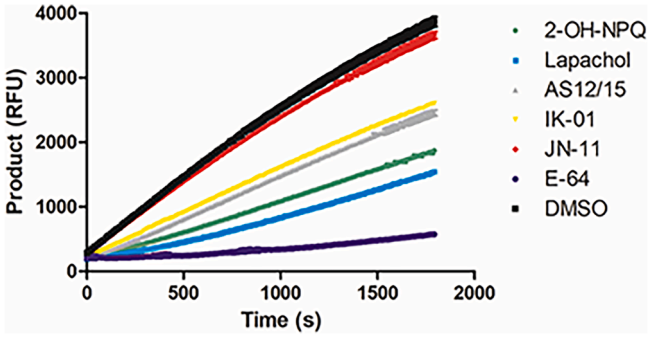

Fig. 9. Reversibility assay. *Following the dilution, product formation was monitored for 30 min. Compound **JN-11**, the most potent naphthoquinone compound (red), recovered the full enzyme activity, while compounds **2-OH-NPQ** (green) and **Lapachol** (cyan) reduced the enzymatic reaction rate by 50% compared to vehicle control (black), while known irreversible inhibitor E-64 (blue) reduced product formation by 90%.*

3. Conclusion

In this work, we reported a rational virtual screening procedure focusing on identifying the most accurate CRZ and RhD structures (for our protocol) and, posteriorly, filtrating a small library of natural and nature-based compounds targeting these proteases. 1,4-Naphthoquinone-based derivatives were identified as promising inhibitors. These molecules were obtained in yields ranging from 39 to 95%, in which all of them were chemically characterized by NMR, melting point, and FTIR techniques. In total, five compounds (**2-OH-NPQ**, **lapachol**, **AS12/15**, **IK-01**, and **JN-11**) exhibited activity against RhD, while three of them (**AS12/15**, **IK-01**, and **JN-11**) were also active toward CRZ. SAR analysis was discussed here. Among these compounds, **JN-11** is highlighted since it demonstrated the best inhibition results for both proteases. Additionally, this compound was further investigated by molecular dynamics, non– and covalent docking simulations. Thus, it was verified that **JN-11** presents good stability in complex with CRZ and RhD proteases at 100 ns simulation. MM-PBSA calculations revealed that van der Waals interactions are more significant forces to stabilize it. Also, it has been seen that **JN-11** presents a high-affinity for RhD, corroborating with its low IC_{50} value. We hypothesized that **JN-11** could undergo a nucleophilic attack by Cys^{25} residue, via a C3-Michael-addition, verified by covalent molecular docking and DFT calculations. Even all results corroborating with literature data, we performed additional experiments to better investigate our proposed mechanism. Thus, time-dependent inhibition and reversibility assays by dilution suggested that **JN-11** is a time-dependent RhD inhibitor but it demonstrated to be a reversible inhibitor. Furthermore, **JN-11** emerges as a promising candidate for the development of a new drug for the treatment of these diseases. However, studies to evaluate effects of **JN-11** in amastigotes and trypomastigotes, as well as investigations into its mechanism of action, are needed to guarantee its safety and efficacy.

4. Materials and methods

4.1. Computational details

The virtual protocol, including molecular docking and dynamics, and DFT calculations were performed on the DELL® Workstation computer, with Intel® Xeon E5-1660 processor, 3.3 GHz, 4 CPUs, NVIDIA® GeForce RTX 2060 graphics card, RAM 8 GB, under the Linux® operating system.

4.2. Virtual screening and study overview

Initially, cysteine proteases' structures from *T. cruzi* and *T. brucei* parasites with co-crystallized inhibitors were used, which were obtained at the RCSB Protein Data Bank – PDB. In total, 26 CRZ (PDB ids: 1AIM, 1EWL, 1EWM, 1EWO, 1EWP, 1F2A, 1F2B, 1F2C, 1F29, 1ME3, 1ME4, 1U9Q, 2AIM, 2OZ2, 3HD3, 3I06, 3IUT, 3KKU, 3LXS, 4KLB, 4PI3, 4QH6, 4W5B, 4W5C, 4XUI, and 6UX6) and 5 RhD (PDB ids: 2P7U, 2P86, 6EX8, 6EXO, and 6EXQ) structures were selected for further analyses in our virtual protocol. In this context, redocking of each co-crystallized inhibitor was performed to identify the most accurate scoring function based on their RMSD values. Then, the best CRZ and RhD redocked poses were selected for further analyses. Posteriorly, a small *in-house* library of 120 natural and nature-based compounds was virtually evaluated upon CRZ and RhD enzymes by using molecular docking simulations. The best ranked compounds were identified, synthesized, and then biologically evaluated on enzymatic assays for their inhibitory effects. Subsequently, the most significant molecular features were revealed by SAR analyses. Compound **JN-11** was identified as a hit compound towards both cysteine proteases. Wherefore, molecular dynamics were performed in order to obtain data concerning the CRZ- and RhD-**JN-11** complexes' stabilities and physicochemical parameters. Concerning their molecular dynamic trajectories, molecular mechanics Poisson-Boltzmann surface (MM-PBSA) calculations were performed to determine such physicochemical parameters, including $\Delta G_{non\text{-}covalent}$. Finally, DFT calculations were performed to investigate (at atomistic level) a hypothesis involving a covalent mechanism of inhibition by **JN-11**, including the $\Delta G^{\ddagger}$ (transition state) energy and conformation. Finally, all procedures and protocols adopted in this study are in accordance with other studies previously published by our research team.[52,59,85–87]

4.3. Target selection and molecular docking simulations

Initially, 26 CRZ structures co-crystallized with inhibitors and 5 RhD structures also containing inhibitors were obtained through the RCSB PDB (http://www.rcsb.org/). For all of them, hydrogen atoms were added, while water molecules and co-crystallized inhibitors were removed. Subsequently, re-docking simulations were performed for each inhibitor into their corresponding target. This procedure was performed using the GOLD® v. 5.8.1 software (https://www.ccdc.cam.ac.uk/solutions/csd-discovery/Components/Gold/). For the re-docking procedures were used Chemical Piecewise Linear Potential (ChemPLP), GoldScore, ChemScore, and Astex Statistical Potential (ASP) scoring functions. Then, the best binding poses were chosen, and their Root-Mean-Square Deviation (RMSD) values were determined using the PyMol® software (https://pymol.org/2/). Posteriorly, a heatmap was generated in the Microsoft Excel® 2016, in which the scoring function that resulted in the lowest RMSD value was considered as the most accurate one. Thus, the best CRZ (PDB id: 1AIM) and RhD (PDB id: 6EXQ) structures were identified and selected for further analyses in our protocol. Simultaneously, a small *in-house* library of natural and nature-based compounds was drawn and converted into 3D-structures using the Argus Lab v. 4.0.1 (http://www.arguslab.com/arguslab.com/ArgusLab.html). Also, the protonation state calculation at pH 5.5 was carried out on MarvinSketch® (https://chemaxon.com/products/marvin) for all these ligands. Then, ten conformations were generated for every ligand, resulting in the choice of the most stable of them (those exhibiting the lowest energy values). Therefore, all compounds were energetically minimized by semi-empirical calculations using PM3 (Parametric Model 3), also on the Argus Lab® v. 4.0.1 software. Finally, GOLD® software was used to perform all docking simulations, in which a 6 Å region surrounding the co-crystallized ligand was selected as a search box. Then, ten different binding poses were generated for all compounds, and the highest FitScore value ($\geq$53.0) was used to select the most promising molecules to be synthesized and evaluated on enzymatic assays. The hit compound was used for covalent docking simulations to identify a potential covalent mechanism of action. For this purpose, the sulfur atom from the Cys^{25} residue (nucleophile) and electrophilic groups from ligands were selected as potential

interacting groups. Finally, this step was carried out in accordance with the procedures mentioned above.

4.4. Molecular dynamics simulation

All molecular dynamic simulations were performed using the GROMACS® v. 2018.3 software (http://www.gromacs.org/). The CRZ- and RhD-ligand complexes were obtained after molecular docking simulations, previously described. Water molecules were removed, while all charges and hydrogen atoms were added using the *DockPrep* module from the Chimera® v. 1.15 software (https://www.cgl.ucsf.edu/chimera/download.html). The CHARMM36 force field was applied to the protein, followed by the TIP3P solvation method. Topologies of ligands were generated by SwissParam® web software (http://www.swissparam.ch/). The protein–ligand complex was added to a 1.0 nm triclinic box, including water molecules and ions at physiological concentration. Subsequently, the system was initially minimized in 10,000 steps by the conjugate gradient method, followed by the system's total minimization to 20,000 steps. NVT (constant number of particles, volume, and temperature) and NPT (constant number of particles, pressure, and temperature) balances were performed at 300 K for 10 ns. With the system assembled, simulations were performed at 100 ns, with non– and complexed proteins. At the end of the simulation time, the most stable conformation was chosen using the MD movie in Chimera® software by performing cluster analyses. RMSD, root-mean-square fluctuation (RMSF), the radius of gyration (Rg), and solvent-accessible surface area (SASA) graphics were generated using the Xmgrace® software (https://math.nyu.edu/aml/software/xmgrace.html). Furthermore, the stereochemical quality of the most stable conformations was analyzed via Ramachandran plot, using the *procheck* module from the SAVES® web software (https://saves.mbi.ucla.edu/). Finally, covalent molecular docking simulations were performed following the same aforementioned procedures, also using the GOLD® v. 5.8.1 software. In this context, both C3– and *C*2-Michael-addition were investigated for their covalent score values.

4.5. MM-PBSA calculations

The MM-PBSA (Molecular Mechanics Poisson-Boltzmann Surface) method is used to calculate the energy values from interactions between ligand and protein. This method calculates the binding free energy ($\Delta G_{binding}$) based on van der Waals and electrostatic interactions (unbound) between the ligand and its receptor during a molecular dynamics simulation.[88] MM-PBSA calculations were performed using trajectories from molecular dynamics at 100 ns using the *g_mmpbsa* module from the GROMACS® software.[89] The $\Delta G_{binding}$ value was determined as the average of the interaction and solvation free energy during the simulation.[88]

4.6. Atomistic covalent mechanism for ***JN-11*** into the active site from rhodesain by DFT calculations

All geometry optimizations were carried out using the B3LYP functional along with the 6–31 + G* basis set. Solvent effects were considered for optimization by using water as an implicit solvent using the solvent model 8 (SM8) from Spartan v. 14 (https://www.wavefun.com/spartan-latest-version). The intrinsic reaction coordinate (IRC) calculations were performed to study, at the atomistic level, forward and reverse reactions through the transition structure (TS), connecting the reactants to the products and *vice-versa*.[18,36] Final points obtained from the IRC calculations were used as initial coordinates for optimizations of local minima.[18,36] Moreover, thermodynamic parameters at 298 K were also useful to determine the zero-point energy (ZPE).[36,59,90] Then, this value was used as a correction factor for local minima.[90,91] All relative energy values are admitted as Gibbs free energy (ΔG), computed using unscaled frequencies.[36] Finally, the electrostatic and steric effects of the protein environment surrounding the active site were completely ignored.[36,59,90]

4.7. Synthesis and characterization of Naphthoquinone-based compounds

Some naphthoquinones were purchased from Sigma-Aldrich (USA) with high purity degree and were used without purification; these included: 1,4-naphthoquinone core, 2,3-dichloro-1,4-naphthoquinone **(2,3-Cl-NPQ)**, 2-bromo-1,4-naphthoquinone **(2-Br-NPQ)**, lawsone or 2-hydroxy-1,4-naphthoquinone **(2-OH-NPQ)**, and 2-methoxy-1,4-naphthoquinone **(2-OCH$_3$-NPQ)**. In contrast, lapachol (2-hydroxy-3-(3-methyl-2-butenyl)-1,4-naphthoquinone) was isolated from the bark of *Tabebuia* sp. tree, collected in the Agreste Region of Alagoas State (Brazil). Still, it was used as starting material for the synthesis of *N*'-(4-hydroxy-3-(3-methylbut-2enyl)-2-oxonaphthalen-1(2*H*)-ylidene)thiosemi-carbazide **(AS12/15)** and *N*'-(4-hydroxy-3-(3methylbut-2-enyl)-2-oxonaphthalen-1(2*H*)-ylidene)isonicotinoylhydrazide **(IK-01)**. The lawsone **(2-OH-NPQ)** was used for the synthesis of *N*'-(4-hydroxy-2oxonaphthalen-1(2*H*)-ylidene)isonicotinoylhydrazide **(JN-22)**, *N*'-(1,4-dihydro-1,4dioxonaphthalen-2-yl)isonicotinoyl hydrazide **(CR-70)**. Finally, 1,4-naphthoquinone core was utilized to prepare 2-(phenylamino) naphthalene-1,4-dione **(JN-08)**, 2-(4methoxyphenylamino) naphthalene-1,4-dione **(JN-17)**, 2-[*N*-(pyridin-2yl)sulfanilamide)] naphthalene-1,4-dione **(JN-11)**, 2-[*N*-(5-methylisoxazol-3yl)sulfanilamide)]naphthalene-1,4-dione **(JN-13)**, and 2-(*N*-benzyl-*N*-methylamino)naphthalene-1,4dione **(JN-16)**.

Melting points were determined by the MQAPF-301® apparatus and were uncorrected. Infrared spectra were obtained using the Bomem® FTIR MB-102 spectrometer with KBr pellets. ^{1}H NMR (400 MHz) and ^{13}C NMR (100 MHz) spectra were recorded using the Bruker Advanced® DPX spectrometer, utilizing $CDCl_3$ or DMSO-d_6 as analytical solvents. Column chromatography was performed using silica gel 60G 0.063–200 mm (70–230 mesh ASTM) Merck® and silica gel 60G 0.2–0.5 mm VETEC®. TLC analyses were performed on precoated aluminum plates of silica gel 60F 254 plates (0.25 mm, Merck®). Solvents were purified and dried according to the standard procedure. For retention time (R_T) and purity degree (%) of all compounds, a Shimadzu® HPLC chromatograph, model SIL-20AHT, was used with a Luna® 5 μm C18(2) 100 Å column (250 × 4.6 mm) and wavelength (λ) of 254 nm (photo diode array (PDA) detector). During all HPLC analyzes, a mixture of methanol/trifluoroacetic acid HPLC degrees (≥99%) was utilized as a mobile phase (v/v 99.9:0.1%). Furthermore, some parameters were established as (*i*) sample concentration of 1 mg/mL, (*ii*) flow rate of 1 mL/min, (*iii*) run time of 10 min, and (*iv*) injection volume of 5 μL. Lastly, R_T and absorbance values were computed in minutes (min) and milli-absorbance unities (mAU). All spectra and chemical characterization data can be found in the Supplementary Material of this manuscript.

Finally, all experimental procedures described in here are in accordance with studies of previously published by our research team.[52,55,57,92]

4.7.1. Extraction and characterization of lapachol

Lapachol was isolated from wooden chips of *Tabebuia* sp. bark by aqueous sodium carbonate extraction (10% w/v), followed by dilute hydrochloric acid precipitation and then ethanol or ethyl acetate recrystallization, leading to 1.0–1.5 g (1–2% yield) from the bark. $C_{15}H_{14}O_3$; mp: 139–140 °C; Yellow solid; R_T: 3.59 min; Purity: 99.9%; ^{1}H NMR (400 MHz, $CDCl_3$, ppm): δ 1.69 (3H, *s*), 1.79 (3H, *s*), 3.30 (1H, *d*, J = 7.4 Hz), 5.21 (1H, *m*), 7.34 (1H, *s*, OH), 7.68 (1H, *td*, J = 7.6 and 1.3 Hz), 7.75 (1H, *td*, J = 7.6 and 1.3 Hz), 8.08 (1H, *dd*, J = 7.5 and 1.4 Hz), 8.12 (1H, *dd*, J = 7.6 and 1.3 Hz). ^{13}C NMR (100 MHz, $CDCl_3$, ppm): δ 17.92 (CH_3), 22.62 (CH), 25.79 (CH_2), 119.63 (C and CH), 123.46 (C), 126.07 (CH) 126.77 (CH), 129.41 (C), 132.89 (CH), 133.88 (C), 134.87 (CH), 152.70 (C), 181.70 (C═O), 184.61 (C═O). FTIR (cm^{-1}): 3354 ($_\delta$OH), 2917 (CH_2 and CH_3), 1665 ($_\nu$C = O), 1597 ($_\nu$C = C), 724 (CH_{Ar}). All these data are in accordance with Barbosa and Neto.[93]

4.7.2. Naphthoquinone-based analogs

1-N'-(4-hydroxy-3-(3-methylbut-2-enyl)-2-oxonaphthalen-1(2H)-ylidene) thiosemicarbazide **(AS12/15)**.

A suspension of 484.1 mg (2.0 mmol) lapachol in 20.0 mL of water was added to 20.0 mL of 0.1 M NaOH, yielding a dark red solution. An aqueous-methanolic (50%) solution of thiosemicarbazide (2.4 mmol; 10.0 mL) was added dropwise to the above solution with constant stirring. The mixture was stirred for 54 h, after which time the solution was neutralized with 10% HCl solution. The crude precipitated product was filtered and washed with cold water. The resulting solid was purified by column chromatography using ethyl acetate and *n*-hexane as eluent in mixture with increasing polarity to give 283.6 mg (45% yield) the thiosemicarbazone **AS12/15** and starting material lapachol. $C_{16}H_{17}N_3O_2$; mp: 174–175 °C; Brown solid; R_T: 5.35 min; Purity: 98.8%; ^{1}H NMR (400 MHz, $CDCl_3$, ppm): δ 1.62 (1H, *s*), 1.74 (1H, *s*), 3.40 (2H, *br s*), 5.09 (1H, *m*), 7.53 (2H, *br s*), 7.97 (1H, *br s*), 8.61 (1H, *br s*), 8.95 (1H, *br s*), 9.21 (1H, *br s*), 14.93 (1H, *br s*). ^{13}C NMR (100 MHz, $CDCl_3$, ppm): δ 17.87 (CH_3), 21.13 (CH_3), 25.44 (CH_2), 117.36 (C), 121.98 (CH), 123.76 (CH), 124.23 (CH), 127.04 (C), 128.80 (CH), 129.49 (C═N), 129.92 (CH), 131.13 (C), 131.25 (C), 155.38 (C), 179.48 (C═S and C═O). FTIR (cm^{-1}): 3485 ($_\nu NH_2$), 3355 ($_\nu NH$), 3141 (CH_2 and CH_3), 1591 ($_\nu C=O$), 1587 and 1435 ($_\nu C=C$), 1286 ($_\nu C=S$), 1172 ($_\nu C$-N), 858 ($_\nu C=S$), 761 (CH_{Ar}). All these data are in accordance with Souza *et al.*[57] and Chikate & Padhye.[94]

1-N'-(4-hydroxy-3-(3-methylbut-2-enyl)-2-oxonaphthalen-1(2H)-ylidene)isonicotinohydrazide **(IK-01)**.

Lapachol (484.1 mg, 2.0 mmol) was dissolved in 20.0 mL of 10% Et_3N solution. To this solution, 5.0 mL of an aqueous solution of isonicotinoylhydrazide (822.8 mg, 6.0 mmol) was added and was kept under constant stirring at room temperature. After 48 h, TLC consumption of the starting material was observed and the reaction was treated with 4.0 mL of glacial acetic acid. A solid was obtained by the precipitation of the medium using ice water; this was filtered and recrystallized from ethanol to obtain 686.2 mg (95% yield) of **IK-01**. $C_{22}H_{20}N_3O_3$; mp: 164–167 °C; Orange solid; R_T: 3.30 min; Purity: ~95%; ^{1}H NMR (400 MHz, DMSO-d_6, ppm): δ 1.62 (3H, *s*), 1.73 (3H, *s*), 3.24 (2H, *d*, J = 6.5 Hz), 5.08 (1H, *m*), 7.54 (2H, *br s*), 7.86 (2H, *d*, J = 5.5 Hz), 7.98 (1H, *br s*), 8.10 (1H, *br s*), 8.90 (2H, *d*, J = 5.5 Hz), 16.4 (1H, *br s*). ^{13}C NMR (100 MHz, DMSO-d_6, ppm): δ 18.41 (CH_3), 21.64 (CH_2), 25.92 (CH_3), 117.92 (C), 122.21 (CH), 122.77 (CH), 123.83 (CH), 124.75 (CH), 128.43 (C═N), 129.94 (CH), 130.88 (CH), 131.48 (CH), 131.79 (C), 140.79 (C), 150.68 (CH), 166.93 (C-OH and NHC = O), 180.17 (C═O). FTIR (cm^{-1}): 3438 ($_\nu NH$), 2983 and 2917 (CH_2 and CH_3), 1672 ($_\nu C=O$), 1593 and 1429 ($_\nu C=C_{Ar}$), 1240 ($_\nu C$–N), 698 (CH_{Ar}). All these data are in accordance with Cardoso *et al.* (2018).[55]

2-N'-(1,4-dihydro-1,4-dioxonaphthalen-2-yl)isonicotinohydrazide **(CR-70)**.

Lawsone **(2-OH-NPQ)** (2.5 g, 14.4 mmol) was dissolved in 100.0 mL of 80% glacial acetic acid solution. To this suspension, 1.6 g (11.7 mmol) of isonicotinoyl hydrazide was added gradually. After the addition of the hydrazide, a color change was observed from yellow to red. After 72 h of constant stirring at room temperature, the solid obtained was filtered off, washed with 80% acetic acid solution and water, dried, and recrystallized from methanol to give 1.8 g (45% yield) of **CR-70**. $C_{16}H_{11}N_3O_3$; Degradation point: 222–224 °C; Orange solid; R_T: 3.39 min; Purity: 96.9%; ^{1}H NMR (400 MHz, DMSO-d_6, ppm): δ 5.76 (1H, *s*), 7.76 (1H, *td*, J = 7.3 and 1.4 Hz), 7.85–7.83 (3H, *m*), 7.94 (2H, *dd*, J = 7.7 and 1.2 Hz), 8.03 (1H, *dd*, J = 7.4 and 1.2 Hz), 8.8 (2H, *d*, J = 5.9 Hz), 9.59 (1H, *s*), 11.05 (1H, *br s*). ^{13}C NMR (100 MHz, DMSO-d_6, ppm): δ 102.41 (CH), 121.86 (CH), 125.93 (CH), 126.34 (CH), 130.94 (C), 132.88 (C), 133.24 (CH), 135.48 (CH), 139.62 (C), 148.70 (C-NH), 150.95 (CH), 164.43 (NHCO), 181.37 (C═O), 182.74 (C═O). FTIR (cm^{-1}): 3317 and 3249 ($_\nu NH$), 1693 ($_\nu C=O_{amide}$), 1674 and 1635 ($_\nu C=O_{naphthoquinone}$), 1527 and 1493 ($_\nu C=C_{Ar}$), 1259 ($_\nu C$–N), 983 ($_\nu N$-N), 777 ($CH_{Ar}$). All these data are in accordance with Cardoso *et al.*[55] and Rani *et al.*[95]

2-N'-(phenylamino)naphthalene-1,4-dione **(JN-08)**.

1,4-Naphthoquinone (474.1 mg, 3.0 mmol) was dissolved in 60.0 mL of water, and after complete dissolution, it was added to 0.3 mL (325.9 mg, 3.5 mmol) of aniline solution. The mixture was stirred at reflux for 24 h when the TLC consumption of the starting material was observed. Solids obtained were filtered, washed with cold water, dried, and recrystallized with methanol to obtain 598.0 mg (69% yield) of **JN-08**. $C_{16}H_{11}N_{16}NO_2$; mp: 156–160 °C; Dark red solid; R_T: 3.36 min; Purity: 98.9%; ^{1}H NMR (400 MHz, $CDCl_3$, ppm): δ 6.43 (1H, *s*), 7.23 (1H, *t*, J = 7.6 Hz), 7.27 (1H, *br s*), 7.29 (1H, *br s*), 7.43 (2H, *t*, J = 7.9 Hz), 7.68 (1H, *td*, J = 7.5 and 1.4 Hz), 7.77 (1H, *td*, J = 7.5 and 1.4 Hz), 8.11 (2H, *m*). ^{13}C NMR (100 MHz, $CDCl_3$, ppm): δ 103.39 (CH), 122.62 (2CH), 125.64 (CH), 126.17 (CH), 126.55 (CH), 129.71 (2CH), 130.33 (C), 132.36 (CH), 133.20 (C), 134.93 (CH), 137.42 (C), 144.73 (C-NH), 182.06 (C═O), 183.95 (C═O). FTIR (cm^{-1}): 3317 ($_\delta NH$), 1670 and 1641 ($_\nu C=O_{naphthoquinone}$), 1595 and 1446 ($_\nu C=C_{Ar}$), 1244 ($_\nu C$–N), 711 ($CH_{Ar}$). All these data are in accordance with Cardoso *et al.*[55] and Martinez *et al.*[96]

2-[N-(Pyridin-2-yl)sulfanilamide)]naphthalene-1,4-dione **(JN-11)**.

1,4-Naphthoquinone (474.1 mg, 3.0 mmol) was dissolved in 20.0 mL of ethanol and after complete dissolution or suspension formation, it was added 498.1 mg (2.0 mmol) of sulfapyridine. The mixture was stirred at reflux for 24 h when the TLC consumption of the starting material was observed. Solids obtained were filtered, washed with cold water, dried, and recrystallized with ethanol to obtain 765 mg (63% yield) of **JN-11**. $C_{22}H_{16}N_2O_4S$; mp: 259–260 °C; Orange solid; R_T: 2.89 min; Purity: 95.1%; ^{1}H NMR (400 MHz, $CDCl_3$, ppm): δ 6.29 (1H, *s*), 6.87 (1H, *t*, J = 6.1 Hz), 7.17 (1H, *d*, J = 8.8 Hz), 7.54 (2H, *d*, J = 8.8 Hz), 7.73 (1H, *m*), 7.79 (1H, *td*, J = 7.5 and 1.4 Hz), 7.86 (2H, *td*, J = 7.5 and 1.5 Hz), 7.89 (1H, *d*, J = 8.7 Hz), 7.95 (1H, *dd*, J = 7.4 and 0.9 Hz), 7.99 (1H, d, J = 4.4 Hz), 8.05 (1H, *dd*, J = 7.5 and 0.9 Hz), 9.37 (1H, *s*). ^{13}C NMR (100 MHz, $CDCl_3$, ppm): δ 104.15 (CH), 112.61 (CH), 122.65 (CH), 125.47 (2CH), 126.37 (CH), 128.06 (2CH), 128.99 (C), 130.49 (C), 132.42 (CH), 133.07 (C), 135.09 (CH), 140.78 (C) 141.91 (CH), 145.17 (2C-NH), 181.41 (C═O), 183.22 (C═O). FTIR (cm^{-1}): 3440 ($_\nu NH$), 1676 and 1633 ($_\nu C=O_{naphthoquinone}$), 1587 and 1522 ($_\nu C=C_{Ar}$), 1302 ($_\nu S=O$), 1142 ($_\nu C$-N or SO_2), 783 (CH_{Ar}). All these data are in accordance with Lawrence *et al.*[97]

2-[N-(5-Methylisoxazol-3-yl)sulfanilamide)]naphthalene-1,4-dione **(JN-13)**.

1,4-Naphthoquinone (474.1 mg, 3.0 mmol) was dissolved in 20.0 mL of ethanol and after complete dissolution or suspension formation, it was added 506.6 mg (2.0 mmol) of sulfamethoxazole. The mixture was stirred at reflux for 48 h when the TLC consumption of the starting material was observed. Solids obtained were filtered, washed with cold water, dried, and recrystallized with ethanol to obtain 719 mg (59% yield) of **JN-13**. $C_{20}H_{15}N_3O_5S$; mp: 189–191 °C; Orange solid; R_T: 2.91 min; Purity: 97.8%; ^{1}H NMR (400 MHz, DMSO-d_6, ppm): δ 2.30 (3H, *s*), 6.15 (1H, *s*), 6.38 (1H, *s*), 7.62 (1H, *t*, J = 8.8 Hz), 7.8 (1H, *td*, J = 7.5 and 1.0 Hz), 7.85–7.88 (3H, br s), 7.96 (1H, *d*, J = 7.7 Hz), 8.07 (1H, *d*, J = 7.3 Hz), 9.44 (1H, s), 11.4 (1H, *s*). ^{13}C NMR (100 MHz, DMSO-d_6, ppm): δ 12.53 (CH_3), 95.90 (CH), 105.23 (CH), 122.95 (CH), 125.80 (CH), 126.72 (CH), 128.69 (CH), 130.86 (C), 132.71 (C), 133.43 (CH), 134.73 (C), 135.39 (CH), 143.51 (C), 145.20 (C-NH), 157.96 (C), 170.83 (C), 181.70 (C═O), 183.59 (C═O). FTIR (cm^{-1}): 3305 ($_\delta NH$), 1674 and 1612 ($_\nu C=O_{naphthoquinone}$), 1591 and 1413 ($_\nu C=C_{Ar}$), 1300 ($_\nu S=O$), 1167 ($_\nu C$-N or SO_2), 694 (CH_{Ar}). All these data are in accordance with Lawrence *et al.*[97]

2-(1-phenylethylamine)naphthalene-1,4-dione **(JN-16)**.

1,4-Naphthoquinone (474.1 mg, 3.0 mmol) was dissolved in 5.0 mL of dimethylformamide (DMF) and after complete dissolution, it was added to 6.5 mmol of 1-phenylethanamine. The mixture was stirred at 80 °C for 24 h when the TLC consumption of the starting material was observed. The crude was extracted with ethyl acetate and brine, organic phases were evaporated and solids obtained were recrystallized with ethanol to obtain 342.2 mg (39% yield) of **JN-16**. $C_{18}H_{15}NO_2$; mp: 157–158 °C; Dark red crystal; R_T: 3.40 min; Purity: 99.9%; ^{1}H NMR

(400 MHz, DMSO-d_6 ppm): δ 1.53 (3H, *d*, $J = 6.8$ Hz), 4.62 (1H, *m*), 5.48 (1H, *s*), 7.23 (1H, *tt*, $J = 7.1$ and 1.6 Hz), 7.33 (1H, *t*, $J = 7.3$ Hz), 7.41 (1H, *d*, $J = 7.6$ Hz), 7.71 (1H, *td*, $J = 7.3$ and 1.6 Hz), 7.74 (1H, *br s*), 7.79 (1H, *td*, $J = 7.6$ and 1.4 Hz), 7.86 (1H, *dd*, $J = 7.6$ and 0.9 Hz). ^{13}C NMR (100 MHz, DMSO-d_6, ppm): δ 23.05 (CH_3), 51.84 (CH), 101.30 (CH), 125.25 (CH), 125.86 (CH), 126.04 (2CH), 127.07 (CH), 128.53 (2CH), 130.32 (C), 132.27 (CH), 132.77 (C), 134.77 (CH), 143.14 (C), 147.52 (C-NH), 181.38 (C═O), 181.50 (C═O). FTIR (cm^{-1}): 3350 ($_{\nu}$NH), 3057 (CH_{Ar}), 2973 and 2863 (CH_{aliph}), 1674 and 1629 ($_{\nu}C = O_{naphthoquinone}$), 1568 and 1502 ($_{\nu}C = C_{Ar}$), 1246 ($_{\nu}$C–N), 731 ($CH_{Ar}$).

2-N'-(4-methoxy-phenylamino)naphthalene-1,4-dione **(JN-17)**.

1,4-Naphthoquinone (474.1 mg, 3.0 mmol) was dissolved in 20.0 mL of ethanol and after complete dissolution, it was added 762.6 mg (6.2 mmol) of 4-methoxyaniline. The mixture was stirred for 24 h when the TLC consumption of the starting material was observed. Solids obtained were filtered, washed with cold water, dried, and recrystallized with ethanol to obtain 468.9 mg (56% yield) of **JN-17**. $C_{17}H_{13}NO_3$; mp: 157–158 °C; Dark red crystal; R_T: 3.29 min; Purity: 99.9%; ^{1}H NMR (400 MHz, $CDCl_3$, ppm): δ 3.84 (3H, *s*), 6.23 (1H, *s*), 6.96 (d, $J = 8.8$ Hz), 7.21 (d, $J = 8.8$ Hz), 8.11 (t, $J = 6.4$ Hz). ^{13}C NMR (100 MHz, $CDCl_3$, ppm): δ 55.58 (CH_3), 102.54 (CH), 114.94 (2CH), 124.86 (2CH), 126.15 (CH), 126.30 (CH), 130.04 (C), 130.44 (C), 132.20 (CH), 133.41 (C), 134.87 (CH), 145.70 (C-NH), 157.72 (C), 182.17 (C═O), 183.75 (C═O). FTIR (cm^{-1}): 3228 ($_{\delta}$NH), 1678 and 1625 ($_{\nu}C = O_{naphthoquinone}$), 1597 and 1506 ($_{\nu}C = C_{Ar}$), 1296 ($_{\nu}$C–O), 1232 ($_{\nu}$C–N), 721 ($CH_{Ar}$). All these data are in accordance with Martinez *et al.*[96]

1-N'-(4-hydroxy-2-oxonaphthalen-1(2H)-ylidene)isonicotino-hydrazide **(JN-22)**.

Lawsone **(2-OH-NPQ)** (484.0 mg, 2.8 mmol) was dissolved in 20.0 mL of 10% Et_3N solution. To this solution, 5.0 mL of an aqueous solution of isonicotinoyl hydrazide (822.8 mg, 6.0 mmol) was added and was kept under constant stirring at room temperature. After 54 h, TLC consumption of the starting material was observed with the formation of two majority compounds at CCD (eluent 9:1 dichloromethane/methanol), one yellow and other purple. The reaction was treated with ice water and 4.0 mL of glacial acetic acid. An orange solid was obtained by the precipitation of the medium using ice water; this was filtered and recrystallized from ethanol to obtain 489.1 mg (60% yield) of **JN-22**. $C_{16}H_{11}N_3O_3$; Degradation point: 222–224 °C; Orange solid; R_T: 3.16 min; Purity: 96.4%; ^{1}H NMR (400 MHz, DMSO-d_6, ppm): δ 5.93 (1H, *s*, OH), 7.58 (1H, *t*, $J = 7.3$ Hz), 7.64 (1H, *t*, $J = 7.3$ Hz), 7.80 (1H, *d*, $J = 6.0$ Hz), 7.90 (2H, *dd*, $J = 7.4$ and 0.8 Hz), 8.12 (1H, *br s*), 8.87 (2H, *d*, $J = 6.0$ Hz), 16.10 (1H, *br s*). ^{13}C NMR (100 MHz, DMSO-d_6, ppm): δ 104.68 (CH), 121.47 (CH), 123.61 (CH), 124.21 (CH), 127.04 (C═N), 129.56 (CH), 131.30 (CH), 132.36 (2C), 139.54 (C), 150.58 (2CH), 169.82 (C-OH and NHCO), 181.66 (C═O). FTIR (cm^{-1}): 3442 ($_{\nu}$OH or NH), 1678 ($_{\nu}C = O$), 1589 and 1446 ($_{\nu}C = C_{Ar}$), 1265 ($_{\nu}$C–N), 793 (CH_{Ar}).

4.8. Assessment of activity upon cruzain and rhodesain

Recombinant cruzain was expressed and purified as previously described Silva *et al.* 2019.[98] Recombinant rhodesain was generously provided by Conor Caffrey (University of California San Diego). Proteolytic activity was measured by monitoring the cleavage of the fluorescent substrate Z-Phe-Arg-aminomethyl coumarin (Z-FR-AMC), in a Synergy 2 (BioTek®) fluorimeter. All assays were performed in 96-well black plate format, in a final volume of 200 µL, in a buffer solution of 0.1 M sodium acetate pH 5.5 in the presence of 1 mM dithiothreitol, 0.01% Triton X-100, 0.5 nM enzyme, and 2.5 µM of the substrate.[99] The assays were performed with 10 min of pre-incubation of the compounds with the enzyme before the substrate addition. Hit compounds were also tested without incubation to investigate whether they were time-dependent inhibitors. The initial screen was performed with 100 µM of compounds. Two independent experiments were performed for each assay, each in triplicates and monitored for 5 min. Enzymatic activities were calculated based on comparison with a DMSO control, from initial rates of reaction. Trans-Epoxysuccinyl-$_L$-leucylamido(4-guanidino) butane (E64) was used as a positive control. Compounds that inhibited>70% enzyme activity had their IC_{50} determined. Dose-response curves were determined in two independent experiments, each involving at least eight compound concentrations in triplicates. Finally, IC_{50} curves were determined by nonlinear regression analysis using GraphPad Prism® v. 5.0 (https://www.graphpad.com/scientific-software/prism/).

4.9. Reversibility assay

Rhodesain at 100-fold its final assay concentration was incubated with the hits at 10-fold its respective IC_{50} value for 30 min in a volume of 2 µL. This mixture was diluted 100-fold with an assay buffer containing 2.5 µM Z-FR-AMC substrate to a final volume of 200 µL, resulting in a standard concentration of enzyme and 0.1 times the IC_{50} value of hits.[84] Irreversible inhibitor will maintain approximately 10% of enzymatic activity, while a rapidly reversible inhibitor will dissociate from the enzyme to restore approximately 90% of enzymatic activity following the dilution event. Fluorescence intensities of 200 µL-wells were monitored continuously for AMC hydrolysis on Synergy 2 (BioTek®) plate reader for 30 min.

Declaration of Competing Interest

The authors declared that there is no conflict of interest.

Acknowledgments

The authors thank the Coordenação de Aperfeiçoamento de Pessoal de Nível Superior (CAPES), Fundação de Amparo à Pesquisa do Estado de Alagoas (FAPEAL) and the National Council for Scientific and Technological Development (CNPq) for their support to the Brazilian Post-Graduate Programs. Also, the authors thank to Prof. PhD. Thiago Mendonça de Aquino and Prof. PhD. Edson de Souza Bento, both from the Center of Analysis and Research in Nuclear Magnetic Resonance, Chemistry and Biotechnology Institute, Federal University of Alagoas, Maceió 57072-970, Brazil, for providing ^{1}H and ^{13}C NMR spectra for CR-70, AS12/15, and Lapachol. Moreover, the authors also thank the Research Collaboratory for Structural Bioinformatics-Protein Data Bank for providing access to crystallographic structures of the target (available at https://www.rcsb.org/), which allowed us to elaborate illustrations for this article.

Funding

This research was funded by the Brazilian Ministry of Health and Fundação de Amparo à Pesquisa do Estado de Alagoas/SUS Research Program (FAPEAL/PPSUS), with the grant number: 60030000712/2013.

*Declaration **of Interest***

The authors have no relevant affiliations or financial involvement with any organization or entity with a financial interest in or financial conflict with the subject matter or materials discussed in the manuscript. This includes employment, consultancies, honoraria, stock ownership or options, expert testimony, grants or patents received or pending, or royalties.

Appendix A. Supplementary data

Supplementary data to this article can be found online at https://doi.org/10.1016/j.bmc.2021.116213.

References

1 Bentivoglio M, Kristensson K. *Sleeping Sickness. Encycl Neurosci. Published online.* 2009:1067–1073. https://doi.org/10.1016/B978-008045046-9.00065-6.
2 Zani CL, Chiari E, Horizonte B, et al. *Anti-Plasmodial and Anti-Trypanosomal Activity of Synthetic.* 1997;5(12):2185–2192.
3 Braga SFP, Martins LC, da Silva EB, et al. Synthesis and biological evaluation of potential inhibitors of the cysteine proteases cruzain and rhodesain designed by molecular simplification. *Bioorganic Med Chem.* 2017;25(6):1889–1900. https://doi.org/10.1016/j.bmc.2017.02.009.
4 Velásquez AMA, Francisco AI, Kohatsu AAN, et al. Synthesis and tripanocidal activity of ferrocenyl and benzyl diamines against Trypanosoma brucei and Trypanosoma cruzi. *Bioorganic Med Chem Lett.* 2014;24(7):1707–1710. https://doi.org/10.1016/j.bmcl.2014.02.046.
5 Fersing C, Boudot C, Paoli-Lombardo R, et al. Antikinetoplastid SAR study in 3-nitroimidazopyridine series: Identification of a novel non-genotoxic and potent anti-T. b. brucei hit-compound with improved pharmacokinetic properties. *Eur J Med Chem.* 2020;206:1–20. https://doi.org/10.1016/j.ejmech.2020.112668.
6 Bourguignon SC, Castro HC, Santos DO, et al. Trypanosoma cruzi: in vitro activity of Epoxy-α-Lap, a derivative of α-lapachone, on trypomastigote and amastigote forms. *Exp Parasitol.* 2009;122(2):91–96. https://doi.org/10.1016/j.exppara.2009.03.002.
7 Zani CL, Chiari E, Krettli AU, et al. Anti-plasmodial and anti-trypanosomal activity of synthetic naphtho[2,3-b]thiophen-4,9-quinones. *Bioorg Med Chem.* 1997;5(12):2185–2192. https://doi.org/10.1016/S0968-0896(97)00155-7.
8 Marciano D, Llorente C, Maugeri DA, et al. Biochemical characterization of stage-specific isoforms of aspartate aminotransferases from Trypanosoma cruzi and Trypanosoma brucei. *Mol Biochem Parasitol.* 2008;161(1):12–20. https://doi.org/10.1016/j.molbiopara.2008.05.005.
9 Burri C, Brun R. Eflornithine for the treatment of human African trypanosomiasis. *Parasitol Res.* 2003;90(S1):S49–S52. https://doi.org/10.1007/s00436-002-0766-5.
10 Mesu VKBK, Kalonji WM, Bardonneau C, et al. Oral fexinidazole for late-stage African Trypanosoma brucei gambiense trypanosomiasis: a pivotal multicentre, randomised, non-inferiority trial. *Lancet.* 2018;391(10116):144–154. https://doi.org/10.1016/S0140-6736(17)32758-7.
11 Tarral A, Blesson S, Mordt OV, et al. Determination of an Optimal Dosing Regimen for Fexinidazole, a Novel Oral Drug for the Treatment of Human African Trypanosomiasis: First-in-Human Studies. *Clin Pharmacokinet.* 2014;53(6):565–580. https://doi.org/10.1007/s40262-014-0136-3.
12 Kaiser M, Bray MA, Cal M, Bourdin Trunz B, Torreele E, Brun R. Antitrypanosomal Activity of Fexinidazole, a New Oral Nitroimidazole Drug Candidate for Treatment of Sleeping Sickness. *Antimicrob Agents Chemother.* 2011;55(12):5602–5608. https://doi.org/10.1128/AAC.00246-11.
13 Prata A. Clinical and epidemiological aspects of Chagas disease. *Lancet Infect Dis.* 2001;1(2):92–100. https://doi.org/10.1016/S1473-3099(01)00065-2.
14 Rodgers J, Steiner I, Kennedy PGE. Generation of neuroinflammation in human African trypanosomiasis. *Neurol - Neuroimmunol Neuroinflammation.* 2019;6(6), e610. https://doi.org/10.1212/NXI.0000000000000610.
15 Blum JA, Schmid C, Burri C, et al. Cardiac Alterations in Human African Trypanosomiasis (T.b. gambiense) with Respect to the Disease Stage and Antiparasitic Treatment. Boelaert M, ed. *PLoS Negl Trop Dis.*. 2009;3(2):e383. https://doi.org/10.1371/journal.pntd.0000383.
16 Soeiro M de NC, Castro SL de. Screening of Potential anti-Trypanosoma cruzi Candidates: In Vitro and In Vivo Studies. Open Med Chem J. 2011;5:21-30. doi:10.2174/1874104501105010021.
17 Hannaert V. Sleeping sickness pathogen (Trypanosoma brucei) and natural products: Therapeutic targets and screening systems. *Planta Med.* 2011;77(6):586–597. https://doi.org/10.1055/s-0030-1250411.
18 Klein P, Barthels F, Johe P, et al. Naphthoquinones as covalent reversible inhibitors of cysteine proteases—studies on inhibition mechanism and kinetics. *Molecules.* 2020;25(9). https://doi.org/10.3390/molecules25092064.
19 Magalhaes Moreira DR, De Oliveira ADT, De Moraes Teixeira, Gomes PA, et al. Conformational restriction of aryl thiosemicarbazones produces potent and selective anti-Trypanosoma cruzi compounds which induce apoptotic parasite death. *Eur J Med Chem.* 2014;75:467–478. https://doi.org/10.1016/j.ejmech.2014.02.001.
20 Doyle PS, Zhou YM, Hsieh I, Greenbaum DC, McKerrow JH, Engel JC. The Trypanosoma cruzi Protease Cruzain Mediates Immune Evasion. Müller I, ed. PLoS Pathog. 2011;7(9):e1002139. doi:10.1371/journal.ppat.1002139.
21 Engel JC, Doyle PS, Palmer J, Hsieh I, Bainton DF, McKerrow JH. Cysteine protease inhibitors alter Golgi complex ultrastructure and function in Trypanosoma cruzi. *J Cell Sci.* 1998;111(5):597–606.
22 Doyle PS, Zhou YM, Engel JC, McKerrow JH. A Cysteine Protease Inhibitor Cures Chagas' Disease in an Immunodeficient-Mouse Model of Infection. *Antimicrob Agents Chemother.* 2007;51(11):3932–3939. https://doi.org/10.1128/AAC.00436-07.
23 Cazzulo J, Stoka V, Turk V. The Major Cysteine Proteinase of Trypanosoma cruzi: A Valid Target for Chemotherapy of Chagas Disease. *Curr Pharm Des.* 2001;7(12):1143–1156. https://doi.org/10.2174/1381612013397528.
24 Ferreira LG, Andricopulo AD. Targeting cysteine proteases in trypanosomatid disease drug discovery. *Pharmacol Ther.* 2017;180:49–61. https://doi.org/10.1016/j.pharmthera.2017.06.004.
25 Ettari R, Zappalà M, Micale N, et al. Synthesis of novel peptidomimetics as inhibitors of protozoan cysteine proteases falcipain-2 and rhodesain. *Eur J Med Chem.* 2010;45(7):3228–3233. https://doi.org/10.1016/j.ejmech.2010.04.003.
26 Steverding D, Sexton DW, Wang X, Gehrke SS, Wagner GK, Caffrey CR. Trypanosoma brucei: Chemical evidence that cathepsin L is essential for survival and a relevant drug target. *Int J Parasitol.* 2012;42(5):481–488. https://doi.org/10.1016/j.ijpara.2012.03.009.
27 Kerr ID, Wu P, Marion-Tsukamaki R, Mackey ZB, Brinen LS. Crystal Structures of TbCatB and Rhodesain, Potential Chemotherapeutic Targets and Major Cysteine Proteases of Trypanosoma brucei. Tschudi C, ed. *PLoS Negl Trop Dis.*. 2010;4(6):e701. https://doi.org/10.1371/journal.pntd.0000701.
28 Zhai X, Meek TD. Catalytic Mechanism of Cruzain from Trypanosoma cruzi As Determined from Solvent Kinetic Isotope Effects of Steady-State and Pre-Steady-State Kinetics. *Biochemistry.* 2018;57(22):3176–3190. https://doi.org/10.1021/acs.biochem.7b01250.
29 Ettari R, Tamborini L, Angelo IC, et al. Inhibition of rhodesain as a novel therapeutic modality for human African trypanosomiasis. *J Med Chem.* 2013;56(14):5637–5658. https://doi.org/10.1021/jm301424d.
30 Ettari R, Previti S, Tamborini L, Cullia G, Grasso S, Zappalà M. The Inhibition of Cysteine Proteases Rhodesain and TbCatB: A Valuable Approach to Treat Human African Trypanosomiasis. *Mini-Reviews Med Chem.* 2016;16(17):1374–1391. https://doi.org/10.2174/1389557515666160509125243.
31 Scarim CB, Jornada DH, Chelucci RC, de Almeida L, dos Santos JL, Chung MC. Current advances in drug discovery for Chagas disease. *Eur J Med Chem.* 2018;155:824–838. https://doi.org/10.1016/j.ejmech.2018.06.040.
32 Arenas P. Medicine and magic among the Maka indians of the Paraguayan Chaco. *J Ethnopharmacol.* 1987;21(3):279–295. https://doi.org/10.1016/0378-8741(87)90104-8.
33 Carneiro PF, Pinto MCRF, Marra RKF, et al. Synthesis and antimalarial activity of quinones and structurally-related oxirane derivatives. *Eur J Med Chem.* 2016;108:134–140. https://doi.org/10.1016/j.ejmech.2015.11.020.
34 Araújo IAC, de Paula RC, Alves CL, et al. Efficacy of lapachol on treatment of cutaneous and visceral leishmaniasis. *Exp Parasitol.* September 2018;2019(199):67–73. https://doi.org/10.1016/j.exppara.2019.02.013.
35 Morello A, Pavani M, Garbarino JA, et al. Effects and mode of action of 1,4-naphthoquinones isolated from Calceolaria sessilis on tumoral cells and Trypanosoma parasites. *Comp Biochem Physiol Part C Comp.* 1995;112(2):119–128. https://doi.org/10.1016/0742-8413(95)02003-9.
36 Delarmelina M, Greco SJ, Carneiro JW d. M. Single step mechanism for nucleophilic substitution of 2,3-dichloro naphthoquinone using nitrogen, oxygen and sulfur nucleophiles: A DFT approach. Tetrahedron. 2017;73(30):4363-4370. doi:10.1016/j.tet.2017.05.095.
37 Duran-Lengua M, Salas-Sarduy E, Cano-Duran LM, et al. Quinoid compounds cause inhibition of falcipain 2, and arrest Plasmodium falciparum growth in vitro. *Lat Am J Pharm.* 2014;33(4):666–674.
38 Monks TJ, Hanzlik RP, Cohen GM, Ross D, Graham DG. Quinone chemistry and toxicity. *Toxicol Appl Pharmacol.* 1992;112(1):2–16. https://doi.org/10.1016/0041-008X(92)90273-U.
39 Goulart MO, Falkowski P, Ossowski T, Liwo A. Electrochemical study of oxygen interaction with lapachol and its radical anions. *Bioelectrochemistry.* 2003;59(1–2):85–87. https://doi.org/10.1016/S1567-5394(03)00005-7.
40 Ventura Pinto A, Lisboa de Castro S. The Trypanocidal Activity of Naphthoquinones: A Review. *Molecules.* 2009;14(11):4570–4590. https://doi.org/10.3390/molecules14114570.
41 Salas C, Tapia RA, Ciudad K, et al. Trypanosoma cruzi: Activities of lapachol and α- and β-lapachone derivatives against epimastigote and trypomastigote forms. *Bioorg Med Chem.* 2008;16(2):668–674. https://doi.org/10.1016/j.bmc.2007.10.038.
42 Delarmelina M, Daltoé RD, Cerri MF, et al. Synthesis, Antitumor Activity and Docking of 2,3-(Substituted)-1,4-Naphthoquinone Derivatives Containing Nitrogen, Oxygen and Sulfur. *J Braz Chem Soc.* 2015;26(9):1804–1816. https://doi.org/10.5935/0103-5053.20150157.
43 Carneiro PF, do Nascimento SB, Pinto A V., et al. New oxirane derivatives of 1,4-naphthoquinones and their evaluation against T. cruzi epimastigote forms. Bioorg Med Chem. 2012;20(16):4995-5000. doi:10.1016/j.bmc.2012.06.027.
44 Goulart MOF, Zani CL, Tonholo J, et al. Trypanocidal activity and redox potential of heterocyclic- and 2-hydroxy-naphthoquinones. *Bioorg Med Chem Lett.* 1997;7(15):2043–2048. https://doi.org/10.1016/S0960-894X(97)00354-5.
45 O. Salas C, Faundez M, Morello A, Diego Maya J, A. Tapia R. Natural and Synthetic Naphthoquinones Active Against Trypanosoma Cruzi: An Initial Step Towards New Drugs for Chagas Disease. Curr Med Chem. 2011;18(1):144-161. doi:10.2174/092986711793979779.
46 Zani CL, Fairlamb AH. 8-Methoxy-naphtho[2,3-b]thiophen-4,9-quinone, a non-competitive inhibitor of trypanothione reductase. *Mem Inst Oswaldo Cruz.* 2003;98(4):565–568. https://doi.org/10.1590/S0074-02762003000400026.
47 Jorqueira A, Gouvêa RM, Ferreira VF, et al. Oxyrane derivative of α-lapachone is potent growth inhibitor of Trypanosoma cruzi epimastigote forms. *Parasitol Res.* 2006;99(4):429–433. https://doi.org/10.1007/s00436-006-0153-8.
48 Ferreira SB, Salomão K, de Carvalho da Silva F, et al. Synthesis and anti-Trypanosoma cruzi activity of β-lapachone analogues. Eur J Med Chem. 2011;46(7):3071-3077. doi:10.1016/j.ejmech.2011.03.012.
49 Ramírez D, Caballero J. Is It Reliable to Take the Molecular Docking Top Scoring Position as the Best Solution without Considering Available Structural Data? *Molecules.* 2018;23(5):1038. https://doi.org/10.3390/molecules23051038.
50 Mena-Ulecia K, Tiznado W, Caballero J. Study of the Differential Activity of Thrombin Inhibitors Using Docking, QSAR, Molecular Dynamics, and MM-GBSA. Salsbury F, ed. PLoS One. 2015;10(11):e0142774. doi:10.1371/journal.pone.0142774.
51 Gohlke H, Hendlich M, Klebe G. Knowledge-based scoring function to predict protein-ligand interactions. *J Mol Biol.* 2000;295(2):337–356. https://doi.org/10.1006/jmbi.1999.3371.
52 Passos GFS, Gomes MGM, de Aquino TM, et al. Computer-Aided Design, Synthesis, and Antiviral Evaluation of Novel Acrylamides as Potential Inhibitors of E3–E2-E1

Glycoproteins Complex from Chikungunya Virus. *Pharmaceuticals.* 2020;13(7):141. https://doi.org/10.3390/ph13070141.
53 Gillmor SA, Craik CS, Fletterick RJ. Structural determinants of specificity in the cysteine protease cruzain. *Protein Sci.* 1997;6(8):1603–1611. https://doi.org/10.1002/pro.5560060801.
54 Giroud M, Dietzel U, Anselm L, et al. Repurposing a Library of Human Cathepsin L Ligands: Identification of Macrocyclic Lactams as Potent Rhodesain and Trypanosoma brucei Inhibitors. *J Med Chem.* 2018;61(8):3350–3369. https://doi.org/10.1021/acs.jmedchem.7b01869.
55 Cardoso SH, de Oliveira CR, Guimarães AS, et al. Synthesis of newly functionalized 1,4-naphthoquinone derivatives and their effects on wound healing in alloxan-induced diabetic mice. *Chem Biol Interact.* 2018;291:55–64. https://doi.org/10.1016/j.cbi.2018.06.007.
56 Campos VR, dos Santos EA, Ferreira VF, et al. Synthesis of carbohydrate-based naphthoquinones and their substituted phenylhydrazono derivatives as anticancer agents. *RSC Adv.* 2012;2(30):11438. https://doi.org/10.1039/c2ra21514d.
57 Souza MA, Johann S, Lima LAR dos S, et al. The antimicrobial activity of lapachol and its thiosemicarbazone and semicarbazone derivatives. Mem Inst Oswaldo Cruz. 2013;108(3):342-351. doi:10.1590/S0074-02762013000300013.
58 Bourguignon SC, Cavalcanti DFB, de Souza AMT, et al. Trypanosoma cruzi: Insights into naphthoquinone effects on growth and proteinase activity. *Exp Parasitol.* 2011;127(1):160–166. https://doi.org/10.1016/j.exppara.2010.07.007.
59 da Silva-Junior EF, Barcellos Franca PH, Ribeiro FF, et al. Molecular Docking Studies Applied to a Dataset of Cruzain Inhibitors. *Curr Comput Aided Drug Des.* 2017;14(1):68–78. https://doi.org/10.2174/1573409913666170519112758.
60 Khan S, Khan FI, Mohammad T, et al. Exploring molecular insights into the interaction mechanism of cholesterol derivatives with the Mce4A: A combined spectroscopic and molecular dynamic simulation studies. *Int J Biol Macromol.* 2018;111:548–560. https://doi.org/10.1016/j.ijbiomac.2017.12.160.
61 Marques DN, Siqueira AS, Gonçalves EC, Barros NLF, de Souza CRB. Homology modeling and molecular dynamics simulations of a cassava translationally controlled tumor protein (MeTCTP). *Plant Gene.* 2019;19, 100185. https://doi.org/10.1016/j.plgene.2019.100185.
62 Bharadwaj S, Lee KE, Dwivedi VD, Kang SG. Computational insights into tetracyclines as inhibitors against SARS-CoV-2 Mpro via combinatorial molecular simulation calculations. *Life Sci.* 2020;257(April), 118080. https://doi.org/10.1016/j.lfs.2020.118080.
63 Idris MO, Yekeen AA, Alakanse OS, Durojaye OA. Computer-aided screening for potential TMPRSS2 inhibitors: a combination of pharmacophore modeling, molecular docking and molecular dynamics simulation approaches. *J Biomol Struct Dyn.* 2020:1–19. https://doi.org/10.1080/07391102.2020.1792346.
64 Zhang D, Lazim R. Application of conventional molecular dynamics simulation in evaluating the stability of apomyoglobin in urea solution. *Sci Rep.* 2017;7(1):44651. https://doi.org/10.1038/srep44651.
65 Ibis C, Tuyun AF, Ozsoy-Gunes Z, et al. Synthesis and biological evaluation of novel nitrogen- and sulfur-containing hetero-1,4-naphthoquinones as potent antifungal and antibacterial agents. *Eur J Med Chem.* 2011;46(12):5861–5867. https://doi.org/10.1016/j.ejmech.2011.09.048.
66 Tandon VK, Maurya HK. 'On water': unprecedented nucleophilic substitution and addition reactions with 1,4-quinones in aqueous suspension. *Tetrahedron Lett.* 2009;50(43):5896–5902. https://doi.org/10.1016/j.tetlet.2009.07.149.
67 Tandon VK, Maurya HK, Tripathi A, et al. 2,3-Disubstituted-1,4-naphthoquinones, 12H-benzo[b]phenothiazine-6,11-diones and related compounds: Synthesis and Biological evaluation as potential antiproliferative and antifungal agents. *Eur J Med Chem.* 2009;44(3):1086–1092. https://doi.org/10.1016/j.ejmech.2008.06.025.
68 Romeiro NC, Aguirre G, Hernández P, et al. Synthesis, trypanocidal activity and docking studies of novel quinoxaline-N-acylhydrazones, designed as cruzain inhibitors candidates. *Bioorg Med Chem.* 2009;17(2):641–652. https://doi.org/10.1016/j.bmc.2008.11.065.
69 Bursulaya BD, Totrov M, Abagyan R, Brooks CL. Comparative study of several algorithms for flexible ligand docking. *J Comput Aided Mol Des.* 2003;17(11):755–763. https://doi.org/10.1023/B:JCAM.0000017496.76572.6f.
70 Cummings MD, DesJarlais RL, Gibbs AC, Mohan V, Jaeger EP. Comparison of automated docking programs as virtual screening tools. *J Med Chem.* 2005;48(4):962–976. https://doi.org/10.1021/jm049798d.
71 Kontoyianni M, Sokol GS, Mcclellan LM. Evaluation of library ranking efficacy in virtual screening. *J Comput Chem.* 2005;26(1):11–22. https://doi.org/10.1002/jcc.20141.
72 Warren GL, Andrews CW, Capelli A-M, et al. A Critical Assessment of Docking Programs and Scoring Functions. *J Med Chem.* 2006;49(20):5912–5931. https://doi.org/10.1021/jm050362n.
73 Malmstrom RD, Watowich SJ. Using free energy of binding calculations to improve the accuracy of virtual screening predictions. *J Chem Inf Model.* 2011;51(7):1648–1655. https://doi.org/10.1021/ci200126v.
74 Silva-Júnior E, França P, Quintas-Júnior L, et al. Dynamic Simulation, Docking and DFT Studies Applied to a Set of Anti-Acetylcholinesterase Inhibitors in the enzyme β-Secretase (BACE-1): An Important Therapeutic Target in Alzheimer's Disease. *Curr Comput Aided Drug Des.* 2017;13(3):1–9. https://doi.org/10.2174/1573409913666170406150905.
75 Awoonor-Williams E, Walsh AG, Rowley CN. Modeling covalent-modifier drugs. *Biochim Biophys Acta - Proteins Proteomics.* 2017;1865(11):1664–1675. https://doi.org/10.1016/j.bbapap.2017.05.009.
76 Arafet K, Ferrer S, Martí S, Moliner V. Quantum mechanics/molecular mechanics studies of the mechanism of falcipain-2 inhibition by the epoxysuccinate E64. *Biochemistry.* 2014;53(20):3336–3346. https://doi.org/10.1021/bi500060h.
77 Arafet K, Ferrer S, Moliner V. First quantum mechanics/molecular mechanics studies of the inhibition mechanism of cruzain by peptidyl halomethyl ketones. *Biochemistry.* 2015;54(21):3381–3391. https://doi.org/10.1021/bi501551g.
78 Arafet K, Ferrer S, González FV, Moliner V. Quantum mechanics/molecular mechanics studies of the mechanism of cysteine protease inhibition by peptidyl-2,3-epoxyketones. *PCCP.* 2017;19(20):12740–12748. https://doi.org/10.1039/C7CP01726J.
79 Arafet K, Ferrer S, Moliner V. Computational Study of the Catalytic Mechanism of the Cruzain Cysteine Protease. *ACS Catal.* 2017;7(2):1207–1215. https://doi.org/10.1021/acscatal.6b03096.
80 Domingo LR, Saéz JA, Zaragozá RJ, Arnó M. Understanding the Participation of Quadricyclane as Nucleophile in Polar [2σ + 2σ + 2π] Cycloadditions toward Electrophilic π Molecules. *J Org Chem.* 2008;73(22):8791–8799. https://doi.org/10.1021/jo801575g.
81 Valente C, Moreira R, Guedes RC, Iley J, Jaffar M, Douglas KT. The 1,4-naphthoquinone scaffold in the design of cysteine protease inhibitors. *Bioorg Med Chem.* 2007;15(15):5340–5350. https://doi.org/10.1016/j.bmc.2007.04.068.
82 Bruno S, Uliassi E, Zaffagnini M, et al. Molecular basis for covalent inhibition of glyceraldehyde-3-phosphate dehydrogenase by a 2-phenoxy-1,4-naphthoquinone small molecule. *Chem Biol Drug Des.* 2017;90(2):225–235. https://doi.org/10.1111/cbdd.12941.
83 McGovern SL, Caselli E, Grigorieff N, Shoichet BK. A Common Mechanism Underlying Promiscuous Inhibitors from Virtual and High-Throughput Screening. *J Med Chem.* 2002;45(8):1712–1722. https://doi.org/10.1021/jm010533y.
84 Boudreau PD, Miller BW, McCall L-I, et al. Design of Gallinamide A Analogs as Potent Inhibitors of the Cysteine Proteases Human Cathepsin L and Trypanosoma cruzi Cruzain. *J Med Chem.* 2019;62(20):9026–9044. https://doi.org/10.1021/acs.jmedchem.9b00294.
85 Silva-júnior EF, Silva EP, França PH, et al. Design, synthesis, molecular docking and biological evaluation of thiophen-2-iminothiazolidine derivatives for use against Trypanosoma cruzi. *Bioorg Med Chem.* 2016;24(18):4228–4240. https://doi.org/10.1016/j.bmc.2016.07.013.
86 Dantas N, de Aquino TMTM, de Araújo-Júnior JXJX, et al. Aminoguanidine hydrazones (AGH's) as modulators of norfloxacin resistance in Staphylococcus aureus that overexpress NorA efflux pump. *Chem Biol Interact.* 2018;280:8–14. https://doi.org/10.1016/j.cbi.2017.12.009.
87 Das S, da Silva CJ, Silva MDM, et al. Highly functionalized piperidines: Free radical scavenging, anticancer activity, DNA interaction and correlation with biological activity. *J Adv Res.* 2018;9. https://doi.org/10.1016/j.jare.2017.10.010.
88 Sarma H, Mattaparthi VSK. Structure-Based Virtual Screening of High-Affinity ATP-Competitive Inhibitors Against Human Lemur Tyrosine Kinase-3 (LMTK3) Domain: A Novel Therapeutic Target for Breast Cancer. *Interdiscip Sci Comput Life Sci.* 2019;11(3):527–541. https://doi.org/10.1007/s12539-018-0302-7.
89 Kumari R, Kumar R, Lynn A. G-mmpbsa -A GROMACS tool for high-throughput MM-PBSA calculations. *J Chem Inf Model.* 2014;54(7):1951–1962. https://doi.org/10.1021/ci500020m.
90 Marques RA, Gomes AOCV, de Brito MV, et al. Annonalide and derivatives: Semisynthesis, cytotoxic activities and studies on interaction of annonalide with DNA. *J Photochem Photobiol B Biol.* 2018;179. https://doi.org/10.1016/j.jphotobiol.2018.01.016.
91 Silva-Junior EF, Barcellos Franca PH, Quintans-Junior LJ, et al. Dynamic Simulation, Docking and DFT Studies Applied to a Set of Anti-Acetylcholinesterase Inhibitors in the enzyme β-Secretase (BACE-1): An Important Therapeutic Target in Alzheimer's Disease. *Curr Comput Aided Drug Des.* 2017;13(4):266–274. https://doi.org/10.2174/1573409913666170406150905.
92 De Brito WA, Dantas MG, Nogueira FHA, et al. Development and validation of HPLC-DAD and UHPLC-DAD methods for the simultaneous determination of guanylhydrazone derivatives employing a factorial design. *Molecules.* 2017;22(9). https://doi.org/10.3390/molecules22091394.
93 Barbosa TP, Diniz Neto H. Preparação de derivados do lapachol em meio ácido e em meio básico: uma proposta de experimentos para a disciplina de Química Orgânica Experimental. *Quim Nova.* 2013;36(2):331–334. https://doi.org/10.1590/S0100-40422013000200021.
94 Chikate RC, Padhye SB. Transition metal quinone–thiosemicarbazone complexes 3: Spectroscopic characterizations of spin-mixed iron (III) of naphthoquinone–thiosemicarbazones. *Spectrochim Acta Part A Mol Biomol Spectrosc.* 2007;66(4–5):1091–1096. https://doi.org/10.1016/j.saa.2006.05.017.
95 Kavitha Rani PR, Fernandez A, George A, et al. Synthesis, spectral characterization, molecular structure and pharmacological studies of N'-(1, 4-naphtho-quinone-2yl) isonicotinohyWdrazide. *Spectrochim Acta Part A Mol Biomol Spectrosc.* 2015;135:1156–1161. https://doi.org/10.1016/j.saa.2014.07.092.
96 Martinez ST, Silva BV, Pinto AC, Ferreira VF. Silva F de C da. Adição de anilinas à naftoquinona em água e em fase sólida. *Quim Nova.* 2012;35(4):858–860. https://doi.org/10.1590/S0100-40422012000400037.
97 Lawrence HR, Kazi A, Luo Y, et al. Synthesis and biological evaluation of naphthoquinone analogs as a novel class of proteasome inhibitors. *Bioorg Med Chem.* 2010;18(15):5576–5592. https://doi.org/10.1016/j.bmc.2010.06.038.
98 Barbosa da Silva E, Dall E, Briza P, Brandstetter H, Ferreira RS. Cruzain structures: apocruzain and cruzain bound to S -methyl thiomethanesulfonate and implications for drug design. *Acta Crystallogr Sect F Struct Biol Commun.* 2019;75(6):419–427. https://doi.org/10.1107/S2053230X19006320.
99 Pereira GAN, da Silva EB, Braga SFP, et al. Discovery and characterization of trypanocidal cysteine protease inhibitors from the 'malaria box'. *Eur J Med Chem.* 2019;179:765–778. https://doi.org/10.1016/j.ejmech.2019.06.062.